Sarcolemmal Ca^{2+}-entry through L-type Ca^{2+} channels controls the profile of Ca^{2+}-activated Cl^- current in canine ventricular myocytes

Short title: Ca^{2+}-entry controls Ca^{2+}-activated Cl^- current

Balázs Horváth[a,b,*], Krisztina Váczi[a,*], Bence Hegyi[a], Mónika Gönczi[a,c], Beatrix Dienes[a], Kornél Kistamás[a], Tamás Bányász[a], János Magyar[a,d], István Baczkó[e], András Varró[e,f], György Seprényi[g], László Csernoch[a], Péter P. Nánási[a,h], Norbert Szentandrássy[a,h]

* The two first authors have equally contributed.
[a]Department of Physiology, Faculty of Medicine, University of Debrecen, Debrecen, Hungary, H-4012 Debrecen, Nagyerdei krt 98, P.O. Box 22, Hungary.
[b]Faculty of Pharmacy, University of Debrecen, Debrecen, Hungary, H-4012 Debrecen, Nagyerdei krt 98, P.O. Box 22, Hungary.
[c]MTA-DE Momentum, Laboratory of Protein Dynamics, Department of Biochemistry and Molecular Biology, Faculty of Medicine, University of Debrecen, Debrecen, Hungary, H-4012 Debrecen, Nagyerdei krt 98, P.O. Box 22, Hungary.
[d]Division of Sport Physiology, Department of Physiology, Faculty of Medicine, University of Debrecen, Debrecen, Hungary, H-4012 Debrecen, Nagyerdei krt 98, P.O. Box 22, Hungary.
[e]Department of Pharmacology and Pharmacotherapy, Faculty of Medicine, University of Szeged, Hungary, H-6720 Szeged, Dóm tér 12, P.O. Box 427, Hungary.
[f]MTA-SZTE Research Group of Cardiovascular Pharmacology, Hungarian Academy of Sciences, Szeged, Hungary, H-6720 Szeged, Dóm tér 12, P.O. Box 427, Hungary.
[g]Department of Medical Biology, Faculty of Medicine, University of Szeged, H-6720 Szeged, Somogyi Béla utca 4, P.O. Box 427, Hungary.
[h]Department of Dental Physiology and Pharmacology, Faculty of Dentistry, University of Debrecen, Debrecen, Hungary, H-4012 Debrecen, Nagyerdei krt 98, P.O. Box 22, Hungary.

Corresponding author: Norbert Szentandrássy
Department of Physiology, University of Debrecen
H-4012 Debrecen, Nagyerdei krt 98, P.O. Box 22, Hungary.
Phone/Fax: +36-52-255575 / +36-52-255116
E-mail: szentandrassy.norbert@med.unideb.hu

Highlights

- Ca^{2+}-entry via $I_{Ca,L}$ is essential for the activation of $I_{Cl(Ca)}$
- $I_{Cl(Ca)}$ can be activated even in the absence of CICR
- TMEM16A and Bestrophin-3 are expressed on human left ventricular muscle
- TMEM16A and Bestrophin-3 co-localize with each other and with $Ca_v1.2$ channels
- Only BAPTA but not EGTA can buffer effectively $[Ca^{2+}]_{cleft}$

Abstract
Ca^{2+}-activated Cl^- current ($I_{Cl(Ca)}$) mediated by TMEM16A and/or Bestrophin-3 may contribute to cardiac arrhythmias. The true profile of $I_{Cl(Ca)}$ during an actual ventricular action potential (AP), however, is poorly understood.
We aimed to study the profile of $I_{Cl(Ca)}$ systematically under physiological conditions (normal Ca^{2+} cycling and AP voltage-clamp) as well as in conditions designed to change $[Ca^{2+}]_i$. The expression of TMEM16A and/or Bestrophin-3 in canine and human left ventricular myocytes was examined. The possible spatial distribution of these proteins and their co-localization with $Ca_v1.2$ was also studied.
The profile of $I_{Cl(Ca),}$ identified as a 9-anthracene carboxylic acid-sensitive current under AP voltage-clamp conditions, contained an early fast outward and a late inward component, overlapping early and terminal repolarizations, respectively. Both components were moderately reduced by ryanodine, while fully abolished by BAPTA, but not EGTA. $[Ca^{2+}]_i$ was monitored using Fura-2-AM. Setting $[Ca^{2+}]_i$ to the systolic level measured in the bulk cytoplasm (1.1 μM) decreased $I_{Cl(Ca),}$ while application of Bay K8644, isoproterenol, and faster stimulation rates increased the amplitude of $I_{Cl(Ca)}$. Ca^{2+}-entry through L-type Ca^{2+} channels was essential for activation of $I_{Cl(Ca)}$. TMEM16A and Bestrophin-3 showed strong co-localization with one another and also with $Ca_v1.2$ channels, when assessed using immunolabeling and confocal microscopy in both canine myocytes and human ventricular myocardium.
Activation of $I_{Cl(Ca)}$ in canine ventricular cells requires Ca^{2+}-entry through neighboring L-type Ca^{2+} channels and is only augmented by SR Ca^{2+}-release. Substantial activation of $I_{Cl(Ca)}$ requires high Ca^{2+} in the dyadic clefts which can be effectively buffered by BAPTA, but not EGTA.

Keywords: Ca^{2+}-activated Cl^- current; canine cardiomyocytes; action potential voltage-clamp; TMEM16A; Bestrophin-3; human cardiomyocytes

Abbreviations

9-AC	9-anthracene carboxylic acid
AP	action potential
APVC	action potential voltage-clamp
APD_{90}	action potential duration at 90 % of repolarization
BKCa	large-conductance Ca^{2+}-activated K^+ channels
CaT	calcium transient
$Ca_v1.2$	pore forming subunit of L-type Ca^{2+} channel
$[Ca^{2+}]_{cleft}$	Ca^{2+} concentration in the dyadic cleft
$[Ca^{2+}]_i$	intracellular Ca^{2+} concentration in bulk cytoplasm
$[Cl^-]_i$	intracellular Cl^- concentration
CDI	Ca^{2+}-dependent inactivation
CICR	Ca^{2+}-induced Ca^{2+}-release
DAD	delayed afterdepolarization
DAPI	4',6-diamidino-2-phenylindole
DIDS	4,4'-diisothiocyanostilbene-2,2'-disulfonic acid
HEPES	4-(2-Hydroxyethyl)piperazine-1-ethanesulfonic acid
ISO	isoproterenol
$I_{9\text{-}AC}$	9-anthracene carboxylic acid-sensitive current
$I_{Ca,L}$	L-type Ca^{2+} current
$I_{Cl(Ca)}$	Ca^{2+}-activated Cl^- current
I_{Ks}	slow component of delayed rectifier K^+ current
I_{NCX}	Na^+/Ca^{2+} exchange current
I_{NISO}	nisoldipine-sensitive current
LTCC	L-type Ca^{2+} channel
PCC	Pearson correlation coefficient
RyR	ryanodine receptor
SEM	Standard Error of the Mean
SITS	4-acetamido-4'-isothiocyanostilbene-2,2'-disulfonic acid
SR	sarcoplasmic reticulum

1. Introduction

The role of anions in cardiac electrophysiology received far less attention as physiological and pharmacological research has focused mainly on cation channels [1] until the discovery of the cAMP-activated Cl^- current [2, 3]. Anion currents are still less understood regarding their molecular identity, physiological role and biophysical, pharmacological properties [4, 5]. Cl^- channels are divided into four groups according to their gating properties: ligand-gated channels, voltage-gated channels, phosphorylation-regulated cystic fibrosis transmembrane conductance regulator channels and Ca^{2+}-activated Cl^- channels have been identified so far [6].

Intracellular Ca^{2+} concentration ($[Ca^{2+}]_i$) and membrane potential are changing dynamically and characteristically throughout the cardiac cycle [7]. Accordingly, the actual magnitudes of these variables delicately guide the Ca^{2+}-activated Cl^- current ($I_{Cl(Ca)}$) during the ventricular action potential (AP). Moreover, the actual Ca^{2+} concentration in various regions of the cell may also be very variable. Ca^{2+} concentration in the dyadic cleft ($[Ca^{2+}]_{cleft}$) during systole is much higher than in the bulk cytoplasm [8]. Increase in $[Ca^{2+}]_i$ can dramatically shift the voltage-dependence of $I_{Cl(Ca)}$ towards more negative potentials [9]. Thus, the actual $[Ca^{2+}]_{cleft}$ has a crucial role in setting the momentary $I_{Cl(Ca)}$ at any given membrane potential. The other peculiar property of $I_{Cl(Ca)}$, in contrast to other types of ion currents underlying the cardiac AP, is that it can mediate both outward (Cl^- influx) and inward (Cl^- efflux) currents because the reversal potential of Cl^- lays between the resting potential and the overshoot potential of the AP [10]. $I_{Cl(Ca)}$ has been characterized in the heart first in the early 1990s [11] as a Ca^{2+}-activated but 4-aminopyridine insensitive component of the transient outward current [12] contributing to the early (phase-1) repolarization of cardiac cells [10].

Although a number of molecular candidates have been claimed to mediate $I_{Cl(Ca)}$, the molecular identity of the channel protein still remains to be elucidated [6, 10]. Recently a new family of anion channels, the Bestrophins have been discovered and proposed to act as chloride channels, or at least as their Ca^{2+}-sensitive subunits [13]. This field was also highlighted by the identification of TMEM16A (also known as Anoctamin1 or Ano1) as another putative candidate for $I_{Cl(Ca)}$ [14-16]. Moreover, TMEM16A expression was described in murine ventricle and confirmed to be responsible for $I_{Cl(Ca)}$ in ventricular myocytes [17].

According to results obtained in rabbit myocytes, activation of $I_{Cl(Ca)}$ required Ca^{2+}-induced Ca^{2+}-release (CICR) from the sarcoplasmic reticulum (SR) in addition to Ca^{2+}-entry through the Ca^{2+} channels of the sarcolemma [11, 18, 19]. Recent publications, however, raised the possibility that activation of $I_{Cl(Ca)}$ is mediated by a Ca^{2+} signal localized at the sarcolemma [20, 21]. Moreover, it has turned out that TMEM16A channels are abundantly available in close proximity to IP_3 receptors in nociceptive neurons and to ryanodine receptors (RyRs) in smooth muscle cells [21, 22].

In the majority of previous studies $I_{Cl(Ca)}$ was recorded under non physiological conditions, i.e. when the Ca^{2+} homeostasis of the myocytes was disturbed, the ionic composition was largely modified and rectangular voltage pulses were applied. These studies have demonstrated the existence of $I_{Cl(Ca)}$ in many species, including rabbit [11, 19], sheep [23], pig [24], and dog [12], however, the role of $I_{Cl(Ca)}$ during the actual AP of the studied ventricular myocyte has not been investigated so far.

$I_{Cl(Ca)}$ can contribute to the development of cardiac arrhythmias. $I_{Cl(Ca)}$ may generate a component of the arrhythmogenic transient inward current, leading to membrane depolarization (delayed afterdepolarization, DAD) and triggered activity in Ca^{2+} overloaded cells [17, 25, 26]. On the other hand, blocking the Cl^- conductance by 9-anthracene carboxylic acid (9-AC) was shown to increase arrhythmia incidence in canine ventricular cells [27].

Therefore the aims of our research were (1) to characterize $I_{Cl(Ca)}$ profiles under actual cardiac APs in canine ventricular cardiomyocytes, in a species with cardiac APs and ion currents most resembling to those of human [28, 29], (2) to study the Ca^{2+}- and rate-dependence of the current, (3) to confirm Cl^- as the charge carrier, (4) to examine the role of transsarcolemmal Ca^{2+}-entry and CICR in activation of $I_{Cl(Ca)}$ (5) to reveal the expression pattern of Bestrophin-3 and TMEM16A and (6) to visualize their cellular appearance regarding co-localization with each other as well as with pore forming subunit of L-type Ca^{2+} channel ($Ca_v1.2$).

Action potential voltage-clamp (APVC) technique was used to record $I_{Cl(Ca)}$ profiles as 9-AC-sensitive current ($I_{9\text{-}AC}$) [30] under various experimental conditions designed to alter intracellular calcium and chloride concentrations. $[Ca^{2+}]_i$ and cell shortening were also monitored. Immunocytochemistry and

confocal imaging were used to detect expression and co-localization of channel proteins in both canine left ventricular myocytes and isolated myocytes and multicellular ventricular preparations obtained from non-diseased human left ventricle. Our results indicate that blockade of SR Ca^{2+}-release may decrease, but fails to eliminate the activation of $I_{Cl(Ca)}$ in canine ventricular cells confirming the critical importance of transsarcolemmal Ca^{2+}-entry through L-type Ca^{2+} channels (LTCCs) in controlling $I_{Cl(Ca)}$. TMEM16A and Bestrophin-3 showed strong co-localization with one another and also with $Ca_v1.2$ channels in both canine and human left ventricular myocardium.

2. Methods

Detailed description of the applied methods including electrophysiological protocols, composition of solutions, molecular biological reagents, etc. is provided in the Supplement.

Human hearts were obtained from organ donors whose non-diseased hearts were explanted to obtain pulmonary and aortic valves for transplant surgery. The investigations conformed to the principles of the Declaration of Helsinki. Experimental protocols were approved by the Ethical Review Board of the Medical Center of the University of Szeged and by the Scientific and Research Ethical Committee of the Medical Scientific Board at the Hungarian Ministry of Health (ETT-TUKEB; No. 51-57/1997 OEj and 4991-0/2010-1018EKU [339/PI/010]). After explantation, each heart was perfused with cardioplegic solution and kept cold (4-6 °C) for 2-4 hours prior to dissection. Cardiac samples were flash-frozen in liquid nitrogen and stored at −80 °C until use. In case of studying cellular expression patterns of ion channel proteins single, isolated left ventricular myocytes were used for immunocytochemistry and confocal imaging.

All animal handling and laboratory procedures conform to the Guide for the Care and Use of Laboratory Animals published by the US National Institutes of Health (NIH publication no. 85-23, revised 1996), and to our Institutional Animal Care and Use Committee approved protocols (license no. 10/2011/DEMÁB). Chemicals and reagents were purchased from Sigma-Aldrich Co. (St. Louis, MO, USA) if not specified otherwise. Ryanodine was obtained from Cayman Chemical Co. (Ann Arbor, MI, USA). All experiments except for molecular biological techniques were applied at 37 °C and pH = 7.4.

Experiments were performed in canine left ventricular myocytes obtained by enzymatic dispersion using the segment perfusion technique [30]. Transmembrane ion currents were recorded using conventional whole-cell voltage clamp and action potential voltage clamp (APVC) techniques. In this latter case the own action potential of the myocyte, recorded previously in current clamp mode in control (in the absence of any drug in the perfusion solution), was played back as a command signal to visualize the actually flowing current profiles. $I_{Cl(Ca)}$ was dissected using 9-AC and presented as $I_{9\text{-}AC}$. Single cell shortening was recorded by optical edge detection, while changes in intracellular free Ca^{2+} concentration were assessed by Fura-2-AM (Molecular Probes, Eugene, OR, USA). Electrical stimulation was applied through the patch pipette to simultaneously record the electrical and the Ca^{2+} signals from the same cell except where otherwise stated. Immunolabeling for TMEM16A, Bestrophin-3 and $Ca_v1.2$ was performed in isolated canine left ventricular myocytes and isolated myocytes and multicellular ventricular preparations obtained from non-diseased human left ventricule, while RyR and cytochrome c levels were studied only in canine cells. Co-localization within pairs of the examined proteins was assessed by off-line image analysis using Pearson correlation coefficient.

All values are presented as arithmetic means ± SEM. Statistical significance of differences was evaluated using one-way ANOVA followed by paired or unpaired Student's t-test as appropriate. Differences were considered significant when p was less than 0.05 and indicated with either asterisks or + symbols.

3. Results

3.1. Ca^{2+}*- and voltage-dependent behavior of* $I_{Cl(Ca)}$ *assessed by conventional voltage-clamp*

$I_{Cl(Ca)}$ was defined as a 9-AC-sensitive current ($I_{9\text{-}AC}$), i.e. as a difference current obtained by measuring the current before and after application of 0.5 mmol/L 9-AC during step depolarizations to a range of voltages from −60 to +60 mV. According to our earlier results, $I_{Cl(Ca)}$ displayed a pronounced increase in its amplitude at membrane potentials positive to −40 mV when normal Ca^{2+} homeostasis was preserved (i.e. when the pipette solution was not buffered for Ca^{2+}) [30]. $I_{Cl(Ca)}$ activated rapidly, but declined to a value close to zero within 20 ms (Fig. 1A). To confirm its dependence on $[Ca^{2+}]_i$, the current was recorded in the presence of two chelators having different Ca^{2+} binding kinetics and affinity. Application of 10 mmol/L BAPTA in the pipette solution without the addition of Ca^{2+} resulted in a great reduction of $I_{Cl(Ca)}$ making the current barely detectable at any test potential (0.07±0.01 A/F at +60 mV, Fig 1B). In contrast, application of 10 mmol/L EGTA in the pipette – although reduced $I_{Cl(Ca)}$ amplitude significantly (from 2.44±0.28 A/F to 1.49±0.27 A/F at +60 mV) – but failed to eliminate the current. In addition, the voltage-dependence of $I_{Cl(Ca)}$ in the presence and absence of EGTA was essentially similar (Fig 1B).
The Ca^{2+}-dependence of $I_{Cl(Ca)}$ was further studied by application of a pipette solution designed to mimic the estimated peak systolic value of $[Ca^{2+}]_i$ (1.1 µmol/L free Ca^{2+}). This was achieved by adding BAPTA and appropriate amounts of Ca^{2+} to the pipette solution (see further details in the Supplement). The amplitude of $I_{Cl(Ca)}$ was significantly larger when $[Ca^{2+}]_i$ was set to 1.1 µmol/L (0.31±0.06 A/F at +60 mV in the 5 cells studied, not shown) comparing to values obtained with 10 mmol/L BAPTA, however, it was much smaller than that measured without buffering $[Ca^{2+}]_i$.
Applying 1 µmol/L nisoldipine, a selective inhibitor of L-type Ca^{2+} channels, further supported the Ca^{2+}-dependent nature of $I_{Cl(Ca)}$, since both L-type Ca^{2+} current ($I_{Ca,L}$) and $I_{Cl(Ca)}$ were eliminated by nisoldipine (Fig. 1C). 9-AC had no influence on the amplitude of $I_{Ca,L}$ in the 5 studied cells (Fig. 1D).
These data are in line with the view that Ca^{2+}-entry through L-type Ca^{2+} channels (in addition to the concomitant Ca^{2+}-release from the SR) may be essential for the physiological activation of $I_{Cl(Ca)}$.

3.2. Influence of preserved Ca^{2+}-homeostasis and buffered $[Ca^{2+}]_i$ on $I_{Cl(Ca)}$ recorded under APVC conditions

The influence of $[Ca^{2+}]_i$ buffering (by EGTA or BAPTA) as well as the preserved Ca^{2+}-homeostasis (no calcium buffering) were further studied on AP configuration and on the simultaneously recorded calcium transients (CaTs). $I_{Cl(Ca)}$ and $I_{Ca,L}$ were studied using their specific blockers (9-AC and nisoldipine, respectively) during the AP applying sequential dissection of ionic currents under conditions of APVC. CaTs were completely abolished when 10 mmol/L of a Ca^{2+} buffer (BAPTA or EGTA) was added to the pipette solution, while characteristic CaTs could be observed without these buffers (Fig. 2A). Importantly, these CaTs recorded in whole-cell configuration without using Ca^{2+} buffers were not different from CaTs elicited with either field stimulation or by injecting current through sharp microelectrodes (data not shown). Under these conditions intracellular Ca^{2+}-handling must be physiological in the absence of intracellular dialysis. In line with these results, unloaded cell shortening was equally abolished by either BAPTA or EGTA (not shown).
Using BAPTA-containing pipette solution resulted in a massive prolongation of APs accompanied by a pronounced positive shift in the plateau potential. Phase-1 amplitude was decreased by both BAPTA and EGTA, this effect was greater in the case of BAPTA than EGTA. In contrast to BAPTA, EGTA failed to increase the duration of APs (Fig. 2B). Similarly, the profile of nisoldipine-sensitive current (I_{NISO}) was strongly different in the presence of the two Ca^{2+} buffers. BAPTA increased both the amplitude and integral of I_{NISO} significantly, while EGTA had no such effect on these parameters (Fig. 2C). On the other hand, I_{NISO} displayed a pronounced early inactivation allowing a second inward peak to rise under Ca^{2+} buffer-free conditions in cells possessing a spike and dome type of AP. This second peak disappeared in the presence of the calcium buffers (Fig. 2C).
9-AC dissected an early narrow outward current (Fig. 2D) having a peak value of 1.62±0.06 A/F which overlapped the phase-1 repolarization of the command AP (appearing 8.1±0.4 ms after the peak of the AP and 7.0±0.9 ms before the end of phase-1 repolarization) (Supplementary Fig. 1). The outward peak always appeared later than the inward peak of I_{NISO} by 6.4±0.5 ms when studied with Sequential Dissection on the same cells using 9-AC followed by nisoldipine (Supplementary Fig. 1). This outward peak of $I_{9\text{-}AC}$ was followed by a smaller late inward current reaching its maximum (−0.16±0.02 A/F) towards the end of the AP. BAPTA reduced significantly both the outward as well

as the inward components of $I_{9\text{-}AC}$ - the outward current peak decreased nearly to zero (See data in Supplementary Table 1). The effect of EGTA on the early outward current peak was smaller (1.17±0.09 A/F, $p<0.05$). These changes in current amplitudes were also reflected by similar alterations of current integrals (Fig. 2D). In summary, CaTs were completely eliminated by both Ca^{2+} buffers, while BAPTA but not EGTA abolished $I_{Cl(Ca)}$ - probably due to a more effective buffering of $[Ca^{2+}]_{cleft}$.

3.3. Effect of changes in $[Cl^-]_i$ on the profile of $I_{Cl(Ca)}$ measured with APVC

In the APVC experiments described above, intracellular Cl^- concentration ($[Cl^-]_i$) was set to 47 mmol/L, yielding a Cl^- reversal potential of −32 mV. In this case, without applying any Ca^{2+} buffer, $I_{9\text{-}AC}$ displayed initially an early outward component which was followed by a late inward component having peak densities of 1.62±0.08 A/F and −0.16±0.03 A/F, respectively, in the 15 cells studied (Fig. 3C and Supplementary Table 1). To test and reinforce the charge carrier, the concentration of Cl^- in the pipette solution was lowered to 27 mmol/L (by replacing Cl^- with equimolar aspartate) setting the new Cl^- reversal potential to −47 mV. This reduction of $[Cl^-]_i$ resulted in an enhancement of the amplitude and integral of the early outward component, while the late inward component was practically eliminated (Fig 3G, H and Supplementary Table 1). Plotting the phase-plane trajectories of $I_{9\text{-}AC}$ revealed that regardless of the actual magnitude of $[Cl^-]_i$ the outward current was the largest within a narrow voltage-range corresponding to phase-1 repolarization of the AP (Fig. 3E, F). These data are considered as further supporting evidence that $I_{Cl(Ca)}$ was indeed mediated by Cl^-.

3.4. Frequency-dependence of $I_{Cl(Ca)}$ during physiological action potentials

$I_{9\text{-}AC}$ profiles were tested at two different steady-state pacing rates under APVC conditions. As reported earlier [30], APD_{90} was increased by 9-AC in a reverse-rate dependent manner (Fig. 4A, B). According to the expectations, both systolic and diastolic $[Ca^{2+}]_i$ were higher when the preparations were stimulated at 2 Hz than at 1 Hz (Fig. 4C). In line with the larger CaT, the density of $I_{9\text{-}AC}$ as well as the total charge carried by the outward component of the current significantly increased when stimulatory frequency was increased from 1 Hz to 2 Hz (Fig. 4D-F and Supplementary Table 1).

3.5. $I_{Cl(Ca)}$ is increased by enhancement of $I_{Ca,L}$

As demonstrated by the experiments displayed in Fig. 1C and Fig. 2, $I_{Ca,L}$ seems to play a critical role in the activation of $I_{Cl(Ca)}$. In the next experiments $I_{Ca,L}$ was enhanced by two different mechanisms. First a protein kinase A-dependent phosphorylation of the channel protein ($Ca_v1.2$) was induced by the β-adrenergic agonist isoproterenol (ISO) applied in a concentration of 10 nmol/L (Fig. 5) [31]. In another set of experiments direct pharmacological stimulation of $I_{Ca,L}$ was achieved by 20 nmol/L of Bay K8644 (Fig. 5) [32]. As it was confirmed with the recording of CaTs, both interventions resulted in an increased systolic calcium concentration, although ISO was more potent in this regard (Fig. 5A, B). ISO acted similarly to Bay K8644: the plateau potential was increased and phase-1 amplitude was reduced by both interventions (Fig. 5C, D). In contrast, opposite effects were observed on the duration of the AP, since AP was shortened by ISO while lengthened by Bay K8644. This can be attributed to the enhancement of the slow delayed rectifier K^+ current (I_{Ks}) by ISO [33]. I_{Ks} is not activated by Bay K8644 but $I_{Ca,L}$ is expected to be increased by both 10 nmol/L ISO and 20 nmol/L Bay K8644. $I_{Cl(Ca)}$ was dissected by 0.5 mmol/L 9-AC using the AP recorded in Tyrode solution as the command signal. Both inward and outward peaks of $I_{9\text{-}AC}$ were significantly larger after pretreatment with either 10 nmol/L isoproterenol or 20 nmol/L Bay K8644 as compared to untreated controls (Fig. 5G). In addition, its profile, its amplitude and the total charge carried by $I_{9\text{-}AC}$ were similar after these pharmacological interventions, irrespective of the way of $I_{Ca,L}$ enhancement (Fig. 5E-H). Enhancement of $I_{Ca,L}$ led to a 2-fold increase in both the outward and the inward components of $I_{9\text{-}AC}$ (Supplementary Table 1). These results support the view that Ca^{2+}-entry through the L-type calcium channels is critically important in the activation of $I_{Cl(Ca)}$.

3.6. Blockade of SR Ca^{2+}-release by ryanodine fails to abolish $I_{Cl(Ca)}$

Contribution of CICR from the SR to the activation of $I_{Cl(Ca)}$ was also examined. Superfusion of the cells with 10 μmol/L ryanodine for 15 min greatly reduced both CaT and cell shortening (Fig. 6A). Ryanodine exposure also resulted in the elevation of the early plateau phase of AP (Fig. 6B, C). However, 0.5 mmol/L 9-AC applied in the presence of ryanodine caused a further reduction of phase-1 amplitude (Fig. 6B, C). Dissection of the corresponding ionic current by 9-AC under APVC conditions using the AP recorded in Tyrode solution as the command signal demonstrated a clear-cut $I_{Cl(Ca)}$ in the presence of ryanodine, having its usual profile, although its amplitude was significantly smaller than that measured under control conditions (Fig. 6D, E, F, and Supplementary Table 1). Taken together, these data give strong support to our hypothesis stating that CICR is not essential for, but contributes to the activation of $I_{Cl(Ca)}$ which is rather influenced by transsarcolemmal Ca^{2+} entry.

3.7. Co-expression of TMEM16A, Bestrophin-3 and $Ca_v1.2$ in the t-tubules of canine left ventricular cells

The expression pattern of potential channel protein candidates of $I_{Cl(Ca)}$ has been studied using immunocytochemistry and confocal microscopy. $Ca_v1.2$, the pore forming subunit of $I_{Ca,L}$, was also assessed. The specificity of the applied antibodies was tested by omitting the primary antibodies during the incubation procedure and also by Western blotting and immunocytochemistry (Supplementary Fig. 2). According to expectations, $Ca_v1.2$ protein expression was most abundant in the t-tubules (Fig. 7A and Supplementary Fig. 3A). Importantly, strong co-localization was found between $Ca_v1.2$ and Bestrophin-3 indicated by the 0.74±0.03 value of the Pearson correlation coefficient (PCC) obtained in 8 cells prepared from 2 animals. TMEM16A showed a similar expression pattern and strong co-localization with Bestrophin-3 (Fig. 7B and Supplementary Fig. 3B) with a PCC of 0.74±0.06 (n=8/2).

3.8. TMEM16A, Bestrophin-3, RyR and cytochrome c expression patterns in canine cardiomyocytes

To exclude the possibility of an accidental co-expression and/or co-localization, the expression of channel protein candidates of $I_{Cl(Ca)}$ was assessed together with other proteins. First the expression of cytochrome c was tested with TMEM16A (Supplementary Fig. 4A). In spite of the recognizable striated pattern of cytochrome c expression, the co-localization of cytochrome c and TMEM16A is unlikely as the merged image did not show strong overlap (PCC was 0.25±0.03 in 7 cells of 2 animals). Although the co-localization of Bestrophin-3 with RyR was slightly stronger (PCC = 0.36±0.05) in 3 cells of 3 animals (See supplementary Fig. 4B), it was much weaker than with $Ca_v1.2$. Similarly, the co-localization of TMEM16A with RyR was not pronounced (PCC of 0.31±0.01) in 3 cells of 1 animal (not shown).

3.9. Co-localization of TMEM16A, Bestrophin-3 and $Ca_v1.2$ in left ventricular tissues and isolated left ventricular cardiomyocytes obtained from non-diseased human hearts

The expression pattern of TMEM16A and Bestrophin-3 has been studied using immunohistochemistry and confocal microscopy. $Ca_v1.2$ protein expression showed a striated pattern suggesting abundant expression in the t-tubules (Fig. 8A and Supplementary Fig. 5A). Similarly to the results obtained in isolated canine myocytes, strong co-localization was found between $Ca_v1.2$ and Bestrophin-3 indicated by the 0.71±0.02 value of PCC obtained in the 7 human cryosections studied. TMEM16A showed a similar expression pattern and strong co-localization with Bestrophin-3 (Supplementary Fig. 5B) with a PCC of 0.80±0.01, n=7). In case of isolated human cells even stronger co-localization was detected than in case of tissue samples or canine cells. PCC for $Ca_v1.2$ and Bestrophin-3 yielded a 0.84±0.02 value obtained in 18 cells prepared from two non-diseased human hearts (Fig. 8A). TMEM16A showed a similar expression pattern and strong co-localization with Bestrophin-3 with a PCC of 0.85±0.02 (n=5/2) (Fig. 8B).

4. Discussion

4.1. Properties of $I_{Cl(Ca)}$

The present study aimed to characterize $I_{Cl(Ca)}$ in isolated canine ventricular myocytes under physiological conditions. This included the application of APVC allowing to record the current during the physiological AP waveform [34] and using pipette solution without buffering of $[Ca^{2+}]_i$ allowing to develop CaTs with normal kinetics. This is critically important in the case of a Ca^{2+}-sensitive current, like $I_{Cl(Ca)}$.

Although several studies described $I_{Cl(Ca)}$ in various cardiac preparations [11, 12, 19, 23, 24, 35], the properties of $I_{Cl(Ca)}$ under true APVC conditions (i.e. when the current is studied during an AP recorded from the same myocyte) have not been analyzed. Furthermore, nonspecific blockers of the current, like 4-acetamido-4'-isothiocyanostilbene-2,2'-disulfonic acid (SITS) and 4,4'-diisothiocyanostilbene-2,2'-disulfonic acid (DIDS) were applied for dissection of $I_{Cl(Ca)}$ in the majority of these studies, which compounds are known to block Na^+ current as well [30]. In the only work performed to study canine cardiac $I_{Cl(Ca)}$ using APVC combined with perforated patch clamp technique a "typical" AP was applied as the command signal and nonspecific blockers were used to dissect $I_{Cl(Ca)}$ [36].

Selectivity of the applied inhibitor, 9-AC is of major importance in this study. It is critical not to alter $I_{Ca,L}$ when a Ca^{2+}-dependent current such as $I_{Cl(Ca)}$ is investigated. Fig. 1D indicates that 0.5 mmol/L 9-AC has no influence on the amplitude of $I_{Ca,L}$. The major K^+ currents, including I_{Kr}, I_{Ks} and I_{K1} were also unaltered by the same dose of 9-AC as we have shown previously [30]. It must be noted, however, that 9-AC was shown to also inhibit Cl^- channels other than the Ca^{2+}-activated ones. Volume regulated Cl^- current was unlikely to be involved in our experiments because the osmolarity of the perfusion fluid was carefully adjusted. 9-AC was shown to reduce ISO-induced cAMP-dependent Cl^- current as well in guinea pig ventricular myocytes [37], but these channels are not expressed in canine [38] and human hearts [39].

$I_{Cl(Ca)}$ was reported to be a rapidly activating and outwardly rectifying transient current having a bell-shaped I-V relation in the range of −40 and +100 mV when studied using rectangular voltage pulses [12]. Our data show that $I_{Cl(Ca)}$, defined as 9-AC-sensitive current, possesses several properties similar to those reported previously under conventional voltage-clamp conditions. (1) $I_{Cl(Ca)}$ began to activate at −20 mV, its amplitude grew with increasing depolarizations having the largest peak around +60 mV, and declined at more positive voltages (not shown, but see Váczi et al. [30]). (2) Time-dependent decay of $I_{Cl(Ca)}$ during these depolarizing pulses, similarly to its activation, was rapid. (3) Activation of $I_{Cl(Ca)}$ required Ca^{2+} since it was abolished in the presence of nisoldipine or 10 mmol/L BAPTA (Fig. 1). (4) Changes of current amplitude with partial replacement of Cl^- by non-permeant anion in the pipette were deducible from the concomitant shift in the Cl^- reversal potential. These similarities were evident in spite of the different experimental conditions.

The profile of $I_{Cl(Ca)}$, when studied as a 9-AC-sensitive current ($I_{9\text{-}AC}$) using APVC, was composed of a fast, early outward and a late inward component. The outward component showed a rapid activation as well as a remarkable rapid decay in spite of the continuously elevated $[Ca^{2+}]_i$ and the existing large driving force for Cl^- influx. One possible explanation for this rapid decay of $I_{Cl(Ca)}$ might be the time dependent inactivation of the channels mediating $I_{Cl(Ca)}$. It had been shown, however, that in the case of a constant $[Ca^{2+}]_i$ $I_{Cl(Ca)}$ showed a time-independent behavior upon prolonged depolarization [12] making this option questionable. The same study also suggested the existence of a low-affinity Ca^{2+} binding site evoking inactivation of $I_{Cl(Ca)}$ [12]. The possible mechanism for Ca^{2+}-dependent inactivation (CDI) was studied in TMEM16A channels expressed in HEK cells, where phosphorylation by a Ca^{2+}-calmodulin dependent protein kinase II was suggested [40]. This however is unlikely to mediate CDI during the AP. A more likely explanation for the rapid decay of $I_{Cl(Ca)}$ may be the rapid and massive reduction of $[Ca^{2+}]_{cleft}$, a change much faster and grater than observed with $[Ca^{2+}]_i$ [41, 42]. This is in line with the co-localized arrangement of the Ca^{2+} and Cl^- channels allowing a direct guidance of $I_{Cl(Ca)}$ by $[Ca^{2+}]_{cleft}$, which is strictly controlled by the neighboring Ca^{2+} channels. Moreover, it was shown that calmodulin can inactivate TMEM16A at $[Ca^{2+}]$ higher than 10 μmol/L at least in HEK cells [43].

The late inward component in the profile of $I_{Cl(Ca)}$ appearing towards the end of the AP also needs discussion. According to our hypothesis the current is activated due to the combination of membrane potential and an appropriate value of $[Ca^{2+}]_{cleft}$ which it is still able to activate $I_{Cl(Ca)}$ but not too high to cause calmodulin dependent inactivation [43]. During terminal repolarization the membrane potential reduces below the equilibrium potential of Cl^- (−32 mV in our experiments except when low $[Cl^-]_i$ was used) therefore an inward current is generated through open channels by the efflux of Cl^-.
The source of the increase of $[Ca^{2+}]_{cleft}$ during diastole can be the spontaneous Ca^{2+}-release through ryanodine receptors in a Ca^{2+}-overloaded cell [44, 45]. The increase of $[Ca^{2+}]_{cleft}$ can result in formation of arrhythmogenic delayed afterdepolarizations (DAD) by forward mode operation of NCX and $I_{Cl(Ca)}$ activation [26]. Activation of $I_{Cl(Ca)}$ in canine ventricular cells [12] as well as in ovine Purkinje cells and ventricular myocytes [46] was responsible for DAD formation highlighting the pathophysiological significance of $I_{Cl(Ca)}$.
However, in a cell without Ca^{2+}-overload increase of $[Ca^{2+}]_{cleft}$ to a level where it can activate $I_{Cl(Ca)}$ at the end of the AP is difficult to explain. One option is the amplification of the window current of Ca^{2+} channels [47, 48] towards the end of the AP due to the growing driving force for Ca^{2+}-influx. $I_{Ca,L}$ mediated Ca^{2+}-influx due to the reactivation of L-type Ca^{2+} channels during terminal repolarization was observed in guinea-pig ventricular myocytes [49]. In some canine ventricular cells a similar late inward peak of I_{NISO} measured in normal Ca^{2+} homeostasis (lack of exogenous Ca^{2+}-buffering) was also present (own unpublished observation).
Another option is the release of Ca^{2+} from myofilaments at the end of the AP [50] which is extruded via NCX and might also lead to the activation of $I_{Cl(Ca)}$. Experimental evidence exists showing this late activation of forward mode NCX at the end of the AP in guinea-pig ventricular cells [49] and also in canine cells [34]. Indeed, we have observed similar timing of this inward I_{NCX} component and the final inward $I_{Cl(Ca)}$ recorded in the same cell (own unpublished observation).
Moreover, late Na^+ current is largest towards the late plateau of the AP measured in APVC during intact Ca^{2+} homeostasis [45]. This Na^+-influx slows down the previously mentioned Ca^{2+}-extrusion via forward mode NCX therefore delays the reduction of $[Ca^{2+}]_{cleft}$ which might also contribute to the activation of $I_{Cl(Ca)}$.
Finally, the late inward component of $I_{Cl(Ca)}$ could be due to the reopening of Cl^- channels at the end of the AP. During the majority of the plateau phase of the AP TMEM16A can be inactive because high $[Ca^{2+}]$ inactivates TMEM16A via calmodulin [43]. Upon the reduction of $[Ca^{2+}]_{cleft}$ Ca^{2+} can gradually dissociate from the low affinity binding site of calmodulin leading to the suspension of CDI of TMEM16A channels. In this scenario $[Ca^{2+}]_{cleft}$ can be large enough to activate $I_{Cl(Ca)}$ but lower than that which causes calmodulin mediated CDI.

4.2. Ca^{2+}-entry via $I_{Ca,L}$ is essential for the activation of $I_{Cl(Ca)}$, while Ca^{2+}-release from SR only augments $I_{Cl(Ca)}$

Previous studies emphasized the principal role of SR Ca^{2+}-release in the activation of $I_{Cl(Ca)}$ in rabbit atrial myocytes and Purkinje fibers [18, 19]. In these studies long lasting (30-60 min) perfusion with ryanodine strongly reduced the amplitude of CaTs eliminating contractions and $I_{Cl(Ca)}$. In contrast, we always observed large amplitude of $I_{Cl(Ca)}$ in canine myocytes in the continuous perfusion of 10 µmol/L ryanodine started 15 min prior to recording (Fig. 6). One might argue that 15 min pretreatment is not enough to achieve the blockade of Ca^{2+}-release from SR but this is unlikely since both CaTs and cell shortening were largely abolished within 8-10 min of ryanodine perfusion (Fig. 6A). Further possible reason for the observed differences in ryanodine-sensitivity of $I_{Cl(Ca)}$ might be the different animal model used or other differences in experimental conditions. We applied canine ventricular cells in the present study in contrast to others using atrial myocytes and Purkinje fibers of the rabbit [18, 19], although in a third study elimination of $I_{Cl(Ca)}$ by ryanodine was reported in conventional voltage-clamp experiments conducted in canine ventricular cells [12]. It is important to note that 9-AC was capable of decreasing phase-1 amplitude even in the presence of ryanodine (Fig. 6B, C). Furthermore, the profile of $I_{Cl(Ca)}$ recorded under APVC conditions in the presence of ryanodine (Fig. 6D) was very similar to that seen without ryanodine (Fig. 3C) further confirming that

in our experimental setting Ca^{2+}-release from the SR is not an absolute requirement for the activation of $I_{Cl(Ca)}$.

In contrast to the limited efficacy of ryanodine to eliminate $I_{Cl(Ca)}$ in our measurements, blockade of Ca^{2+}-entry through LTCCs by nisoldipine fully abolished $I_{Cl(Ca)}$. Previous studies using calcium channel blockers, like cadmium, nisoldipine, and nicardipine described similar results [11, 51]. I_{NISO} peak always occurred earlier than the peak of $I_{Cl(Ca)}$ in our experiments (Supplementary Fig. 1.) further confirming the essential role of Ca^{2+}-entry through LTCCs in the physiological activation of $I_{Cl(Ca)}$. It must be mentioned, however, that I_{NISO} is not exclusively composed of $I_{Ca,L}$ but it also contains all the electrogenic processes which are influenced by Ca^{2+}. The reason for it is that although nisoldipine itself is highly selective for LTCC [34] but it also eliminates the major route of Ca^{2+}-entry to the cell. As a consequence, the trigger for CICR is reduced leading to a drop in both $[Ca^{2+}]_{cleft}$ and $[Ca^{2+}]_i$. Among those Ca^{2+}-dependent processes which could be part of I_{NISO} one can find the current mediated by Na^+/Ca^{2+} exchange (I_{NCX}), Ca^{2+}-dependent K^+ channels, TRP channels and $I_{Cl(Ca)}$ itself. The contribution of $I_{Cl(Ca)}$ is not an issue in our experiments because nisoldipine was applied in the presence of 9-AC therefore $I_{Cl(Ca)}$ has already been eliminated. Ca^{2+}-dependent K^+ channels and TRP channels are unlikely to make a large contribution [52] to I_{NISO} which leaves I_{NCX} as the other main component of I_{NISO}. I_{NCX} can be an outward current leading to Ca^{2+}-influx at the beginning of the cardiac AP but this is limited to a few milliseconds [49, 53]. Na^+/Ca^{2+} exchanger generates mainly an inward current during the cardiac AP [49, 54] which contributes to a smaller or larger extent to I_{NISO}. According to Janvier et al. the two currents (I_{NCX} and $I_{Ca,L}$) have equal contribution to the inward current during the plateau phase of ferret ventricular AP [54]. However, according to results obtained using guinea pig ventricular cells under experimental conditions similar to our current study, the contribution of I_{NCX} to I_{NISO} is much smaller especially during the early phase of AP plateau (only about 25-30%) [49]. During the late plateau the contribution of I_{NCX} and $I_{Ca,L}$ to I_{NISO} becomes roughly equal [54]. In our experiments we observed a substantial prolongation of the AP in the presence of 10 mmol/L BAPTA applied in the pipette solution (Fig. 2B), similarly to what has been described in our earlier study also on canine cells in the presence of 5 μmol/L BAPTA-AM [55]. This is in great contrast with the study of Janvier et al. where the AP became shorter after the application of 5 μmol/L BAPTA-AM [54]. This shortening was explained by the reduction of I_{NCX} and therefore the smaller overall depolarizing drive during the plateau phase in the presence of BAPTA-AM. The enhancement of $I_{Ca,L}$ due to the lack of CDI of LTCC by strong $[Ca^{2+}]_{cleft}$ buffering can lead to the prolongation of the AP as seen in this study (Fig. 2). This phenomenon, however, was not emphasized in the study of Janvier et al. On the contrary, buffering Ca^{2+} increased $I_{Ca,L}$ about eight times compared to the physiological conditions according to modeling results in the guinea pig cells [49]. It seems therefore that the main effect of Ca^{2+}-buffering in canine and guinea-pig cells is the enhancement of $I_{Ca,L}$ whereas in ferret ventricular cells the reduction of I_{NCX} dominates explaining the opposite actions of Ca^{2+}-buffering on the duration of the AP. Our results therefore suggest that I_{NCX} is less dominant in the dog than in ferret but it is more similar to that of guinea pig in the maintenance of AP plateau. Another option is that in case of canine cells the dominant effect of Ca^{2+}-buffering is the increase of $I_{Ca,L}$ resulting in AP prolongation.

Our other experiments support the importance of Ca^{2+}-entry through LTCCs further. The amplitude of $I_{Cl(Ca)}$ strongly increased when $I_{Ca,L}$ was enhanced either by ISO or Bay K8644 (Fig. 5). Both drugs increases $I_{Ca,L}$ but as Bay K8644 does not phosphorylate channel proteins (unlike what is the case in the presence of ISO), direct interaction with the Ca^{2+}-activated Cl^- channels can be excluded in this case. However, both treatments increased $I_{Ca,L}$ (not shown) and $I_{Cl(Ca)}$ amplitudes to the same extent, while the concomitant elevations of CaT amplitudes were not proportional (Fig. 5). In line with this view, increasing the stimulation rate from 1 to 2 Hz also increased $I_{Cl(Ca)}$ probably due to the increased transsarcolemmal Ca^{2+} entry (Fig. 4).

Co-localization studies have revealed that LTCCs and RyRs are in close proximity to one another within the dyadic cleft [56]. During excitation-contraction coupling $[Ca^{2+}]_{cleft}$ is believed to be much higher and has faster kinetics than in the bulk cytoplasm [41, 42]. However, measuring $[Ca^{2+}]_{cleft}$ directly is just becoming available [42, 57]. According to our hypothesis, $I_{Cl(Ca)}$ is controlled locally, by $[Ca^{2+}]_{cleft}$, rather than bulk $[Ca^{2+}]_i$. This approach is supported by the experiments aiming to set $[Ca^{2+}]_i$ to 1.1 μmol/L (which corresponds to peak value of systolic $[Ca^{2+}]_i$) by dialyzing cells with pipette solution containing 1.1 μmol/L of free Ca^{2+}. In this case, $I_{Cl(Ca)}$ amplitude was much smaller,

only 13 % of the value obtained without buffering $[Ca^{2+}]_i$. This is in a good agreement with the Ca^{2+}-sensitivity of $I_{Cl(Ca)}$ determined in murine airway smooth muscle, where the EC_{50} was estimated to be 3.3 µmol/L but only 20-50 µmol/L $[Ca^{2+}]_i$ resulted in full activation of the current [58]. Therefore, the significantly larger $I_{Cl(Ca)}$ measured under physiological conditions, i.e. without buffering $[Ca^{2+}]_i$, is probably due to the higher $[Ca^{2+}]_{cleft}$.

The different actions of EGTA and BAPTA on $I_{Cl(Ca)}$ and $I_{Ca,L}$ can also be explained by the ability of Ca^{2+} chelators to differentially affect $[Ca^{2+}]_i$ and $[Ca^{2+}]_{cleft}$ [59]. These agents suppress $I_{Cl(Ca)}$ and CDI of $I_{Ca,L}$ with different efficacy. Although both buffers eliminated CaTs (Fig. 2A), only BAPTA was effective to suppress CDI of $I_{Ca,L}$ resulting in significantly higher I_{NISO} amplitude and total charge values (Fig. 2C) in addition to the much longer AP (Fig. 2B). BAPTA fully eliminated $I_{Cl(Ca)}$ during the AP, while EGTA only decreased its amplitude and the total charge carried by the current (Fig. 2D). These results are in a good agreement with the conventional voltage-clamp observations (Fig. 1B). The reason for the different buffering efficacy is that BAPTA has a 100 times faster binding rate to Ca^{2+} than EGTA [59]. Similarly to the present study, effects of the two buffers were compared on large-conductance Ca^{2+}-activated K^+ channels (BKCa) [60]. In line with our findings, namely that $[Ca^{2+}]_{cleft}$ could be buffered by the rapidly acting BAPTA, but not by EGTA, BKCa channels could be activated by Ca^{2+} in the presence of EGTA, while the current was fully abolished by BAPTA [60].

As mentioned previously, blockade of Ca^{2+}-release from the SR failed to fully abolish $I_{Cl(Ca)}$, only some reduction of the current amplitude was observed. It is rather difficult, however, to judge the relative contribution of Ca^{2+}-entry through LTCC and Ca^{2+}-release from SR to the activation of $I_{Cl(Ca)}$. One reason is that the CDI of $I_{Ca,L}$ is known to be reduced when Ca^{2+}-release from SR is blocked (e.g. in the presence of ryanodine). Therefore the relative contribution of LTCCs to $I_{Cl(Ca)}$ activation is probably overestimated in the presence of ryanodine. Determining the precise contribution of these two mechanisms is further complicated by the presence of several other Ca^{2+}-dependent processes involved in the ventricular electrical activity, including the Na^+/Ca^{2+} exchanger, Ca^{2+}-dependent K^+ channels, and various Ca^{2+} pumps, likely to be altered by changes in $[Ca^{2+}]_i$ and even more by alterations in $[Ca^{2+}]_{cleft}$. It would be important, therefore, to measure the $[Ca^{2+}]_{cleft}$ directly in the vicinity of the LTCC and Ca^{2+}-activated Cl^- channels. It must be mentioned however that in this study we only examined the source of Ca^{2+} that activates $I_{Cl(Ca)}$ (via Ca^{2+}-entry from the extracellular space or Ca^{2+} released from the SR) but we did not discriminate the route of Ca^{2+}-entry (via LTCC or reverse mode NCX). The contribution of Ca^{2+}-entry via NCX is unlikely to play a major role if any in activating $I_{Cl(Ca)}$ (note the lack of outward current on I_{NISO} trace on the cell shown on Supplementary Fig. 1) but can not be excluded.

4.3. Co-localization of $Ca_v1.2$ with TMEM16A and Bestrophin-3 proteins, possible contributors of $I_{Cl(Ca)}$

In this study we tested the co-localization of Bestrophin-3 and/or TMEM16A, the two likely candidates responsible for $I_{Cl(Ca)}$ [13-16], with $Ca_v1.2$ protein. The expression of Bestrophin-1 was demonstrated in murine heart. Moreover, when Bestrophin-1 was extracted and transfected to HEK cells, the resultant current recapitulated the characteristics of $I_{Cl(Ca)}$, including Ca^{2+}-dependence, anion selectivity and sensitivity to DIDS or niflumic acid [61]. The same group reported the expression of Bestrophin-3 in murine and human heart (although only at mRNA level in the latter) similarly to Bestrophin-1 [62]. Bestrophin-3, when expressed in HEK cells, was activated by Ca^{2+} with the K_d of 175 nmol/L, and blocked by micromolar concentrations of DIDS and niflumic acid [62]. The cellular expression of Bestrophin-3 in murine ventricular cells showed a punctuated pattern which was strong in the sarcolemma [62]. In our images obtained in canine ventricular myocytes the cellular expression of Bestrophin-3 showed striated pattern rather than being punctuated. Bestrophin-3 expression in human samples (left ventricular myocardium as well as isolated left ventricular cells), similarly to that seen in canine cells, showed striated pattern.

Cardiac expression of TMEM16A has been described in murine ventricle [17], but this is the first report demonstrating it in canine and human ventricular preparations. In both species a clear-cut striated pattern was observed. Importantly, the expression of Bestrophin-3 showed strong co-localization with $Ca_v1.2$ channel protein (Fig. 7A and 8A) and TMEM16A (Fig. 7B and 8B) making it

very likely that $Ca_v1.2$ and TMEM16A also co-localize with one another. In line with the results of the present study Ca^{2+}-activated Cl^- channels localize close to RyR and are controlled by local Ca^{2+} signals in airway smooth muscle [58]. On the contrary to our finding in rat dorsal root sensory neurons TMEM16A channels were reported to be activated by G protein-coupled receptor induced Ca^{2+} release, but not by Ca^{2+}-influx through voltage-gated Ca^{2+} channels [21]. As a mechanism behind this the tethering of TMEM16A- and G protein-coupled receptor-containing, caveolin-1 enriched plasma membrane domains to juxtamembrane regions of the endoplasmic reticulum was mentioned. Here inositol 1,4,5-trisphosphate receptor 1 is the interacting partner of the carboxyl terminus and first intracellular loop of TMEM16A while voltage-gated Ca^{2+} channels are located in other parts of the plasma membrane [21]. On cardiac muscle however caveolin-3 is associated to the same compartment with Cav1.2 proteins among many other [63]. Moreover, in case of hippocampal neurons TMEM16B was reported to appear in close proximity of Ca^{2+} channels and NMDA receptors [64].
In addition, Bestrophins can associate with TMEM16A and contribute to the functional channel in vascular smooth muscle cells [65]. This possibility, however, is very difficult to test since TMEM16A modulates Bestrophin expression [66]. Down-regulation of TMEM16A reduced the expression of Bestrophins, however, a reduced expression of LTCCs has also been mentioned [66]. On the other hand, Bestrophins were shown to form preferentially homomeric channels [67], similarly to TMEM16A [68], which may question the ability of the two proteins to form a single functional ion channel.
The striated pattern of TMEM16A, Bestrophin-3, and $Ca_v1.2$ expression is most likely due to the strong expression of these proteins in the membranes of the t-tubules (Fig. 7 and 8). Similar images were published in murine and human ventricular cardiomyocytes with $Ca_v1.2$ expression in the t-tubules [69]. The accidental co-localization of the channel proteins due to technical factors of imaging is unlikely since the co-localization of TMEM16A with cytochrome c was weak (Supplementary Fig. 4A). Similarly, less pronounced co-localization was seen between Bestrophin-3 and RyR (Supplementary Fig. 4B) than between Bestrophin-3 and TMEM16A/$Ca_v1.2$ (Fig. 7 and 8). The expression pattern of RyR was very similar to that seen in rat ventricular myocytes [70]. The co-localization of $Ca_v1.2$ with RyR and RyR with $Ca_v1.2$ was approximately 57 and 37 %, respectively, in adult rat ventricular myocytes [55].

4.4. Summary

The major finding of the present study was to show that Ca^{2+}-entry through LTCC is sufficient for the activation of $I_{Cl(Ca)}$ and does not require Ca^{2+}-release from the SR through RyR. Our results demonstrate the expression of Bestrophin-3 and TMEM16A in both canine and human ventricular preparations for the first time and the strong co-localization of Bestrophin-3 with TMEM16A and $Ca_v1.2$ protein. Elucidation of the exact roles of TMEM16A and/or Bestrophin-3 in the formation of $I_{Cl(Ca)}$, however, requires further studies.

Funding

This work was supported by the Hungarian Scientific Research Fund (OTKA-PD101171 to NS, OTKA-K100151 and OTKA-K115397 to PPN, OTKA-K101196 to TB, OTKA-K109736 to JM, OTKA-NK104331 to BH, PPN, IB and AV, and OTKA-K109610 to IB), the Hungarian Academy of Sciences, the Hungarian Government (TÁMOP-4.2.2.A-11/1/KONV-2012-0045 to all authors except for MG, BD, LC, IB and AV), the János Bolyai Research Scholarship of the Hungarian Academy of Sciences to MG and NS and the University of Debrecen (RH/751/2015 to NS).
Funding sources had no involvement in preparation of the article; in study design; in the collection, analysis and interpretation of data; in writing of the report; and in the decision to submit the article for publication.

Acknowledgment

The authors thank Miss Éva Sági for her excellent technical assistance. The support of the Momentum program (LP2012-41) of the Hungarian Academy of Sciences is gratefully acknowledged.

Disclosure statement
None.

Conflict of interest statement
None.

References

1. Adkins GB, Curtis MJ. Potential role of cardiac chloride channels and transporters as novel therapeutic targets. Pharmacol Ther 2015; 145: 67-75. doi: 10.1016/j.pharmthera.2014.08.002
2. Bahinski A, Nairn AC, Greengard P, Gadsby DC. Chloride conductance regulated by cyclic AMP-dependent protein kinase in cardiac myocytes. Nature 1989; 340: 718-21. doi: 10.1038/340718a0
3. Harvey RD, Hume JR. Autonomic regulation of a chloride current in heart. Science 1989; 244: 983-5. doi: 10.1126/science.2543073
4. Jentsch TJ, Stein V, Weinreich F, Zdebik AA. Molecular structure and physiological function of chloride channels. Physiol Rev 2002; 82: 503-68. doi: 10.1152/physrev.00029.2001
5. Duran C, Thompson CH, Xiao Q, Hartzell HC. Chloride channels: often enigmatic, rarely predictable. Annu Rev Physiol 2010; 72: 95-121. doi: 10.1146/annurev-physiol-021909-135811
6. Eggermont J. Calcium-activated chloride channels: (un)known, (un)loved? Proc Am Thorac Soc 2004; 1: 22-7. doi: 10.1513/pats.2306010
7. Bers DM. Calcium cycling and signaling in cardiac myocytes. Annu Rev Physiol 2008; 70: 23-49. doi: 10.1146/annurev.physiol.70.113006.100455
8. Bers DM. Cardiac excitation-contraction coupling. Nature 2002; 415: 198-205. doi: 10.1038/415198a
9. Zhang S, Chen Y, An H, Liu H, Li J, Pang C, et al. A novel biophysical model on calcium and voltage dual dependent gating of calcium-activated chloride channel. J Theor Biol 2014; 355: 229-35. doi: 10.1016/j.jtbi.2014.04.004
10. Hartzell C, Putzier I, Arreola J. Calcium-activated chloride channels. Annu Rev Physiol 2005; 67: 719-58. doi: 10.1146/annurev.physiol.67.032003.154341
11. Zygmunt AC, Gibbons WR. Calcium-activated chloride current in rabbit ventricular myocytes. Circ Res 1991; 68: 424-37. doi: 10.1161/01.RES.68.2.424
12. Zygmunt AC. Intracellular calcium activates a chloride current in canine ventricular myocytes. Am J Physiol 1994; 267: H1984-95.
13. Sun H, Tsunenari T, Yau KW, Nathans J. The vitelliform macular dystrophy protein defines a new family of chloride channels. Proc Natl Acad Sci U S A 2002; 99: 4008-13. doi: 10.1073/pnas.052692999
14. Caputo A, Caci E, Ferrera L, Pedemonte N, Barsanti C, Sondo E, et al. TMEM16A, a membrane protein associated with calcium-dependent chloride channel activity. Science 2008; 322: 590-4. doi: 10.1126/science.1163518
15. Yang YD, Cho H, Koo JY, Tak MH, Cho Y, Shim WS, et al. TMEM16A confers receptor-activated calcium-dependent chloride conductance. Nature 2008; 455: 1210-5. doi: 10.1038/nature07313
16. Schroeder BC, Cheng T, Jan YN, Jan LY. Expression cloning of TMEM16A as a calcium-activated chloride channel subunit. Cell 2008; 134: 1019-29. doi: 10.1016/j.cell.2008.09.003
17. Ye Z, Wu MM, Wang CY, Li YC, Yu CJ, Gong YF, et al. Characterization of Cardiac Anoctamin1 Ca -activated Chloride Channels and Functional Role in Ischemia-Induced Arrhythmias. J Cell Physiol 2015; 230: 337-46. doi: 10.1002/jcp.24709
18. Zygmunt AC, Gibbons WR. Properties of the calcium-activated chloride current in heart. J Gen Physiol 1992; 99: 391-414. doi: 10.1085/jgp.99.3.391
19. Sipido KR, Callewaert G, Carmeliet E. [Ca2+]i transients and [Ca2+]i-dependent chloride current in single Purkinje cells from rabbit heart. J physiol 1993; 468: 641-67. doi: 10.1113/jphysiol.1993.sp019793
20. Jin X, Shah S, Du X, Zhang H, Gamper N. Activation of Ca -activated Cl channel ANO1 by localized Ca2+ signals. J physiol 2016; 594: 19-30. doi: 10.1113/jphysiol.2014.275107
21. Jin X, Shah S, Liu Y, Zhang H, Lees M, Fu Z, et al. Activation of the Cl- channel ANO1 by localized calcium signals in nociceptive sensory neurons requires coupling with the IP3 receptor. Sci Signal 2013; 6: ra73. doi: 10.1126/scisignal.2004184
22. Zhuge R, Bao R, Fogarty KE, Lifshitz LM. Ca2+ sparks act as potent regulators of excitation-contraction coupling in airway smooth muscle. J Biol Chem 2010; 285: 2203-10. doi: 10.1074/jbc.M109.067546

23. Verkerk AO, Tan HL, Ravesloot JH. Ca2+-activated Cl- current reduces transmural electrical heterogeneity within the rabbit left ventricle. Acta Physiol Scand 2004; 180: 239-47. doi: 10.1111/j.0001-6772.2003.01252.x
24. Li GR, Sun H, To J, Tse HF, Lau CP. Demonstration of calcium-activated transient outward chloride current and delayed rectifier potassium currents in Swine atrial myocytes. J Mol Cell Cardiol 2004; 36: 495-504. doi: 10.1016/j.yjmcc.2004.01.005
25. Szigeti G, Rusznak Z, Kovacs L, Papp Z. Calcium-activated transient membrane currents are carried mainly by chloride ions in isolated atrial, ventricular and Purkinje cells of rabbit heart. Exp Physiol 1998; 83: 137-53. doi: 10.1113/expphysiol.1998.sp004097
26. Zygmunt AC, Goodrow RJ, Weigel CM. INaCa and ICl(Ca) contribute to isoproterenol-induced delayed after depolarizations in midmyocardial cells. Am J Physiol 1998; 275: H1979-92.
27. Fulop L, Fiak E, Szentandrassy N, Magyar J, Nanasi PP, Banyasz T. The role of transmembrane chloride current in afterdepolarisations in canine ventricular cardiomyocytes. Gen Physiol Biophys 2003; 22: 341-53.
28. Szabo G, Szentandrassy N, Biro T, Toth BI, Czifra G, Magyar J, et al. Asymmetrical distribution of ion channels in canine and human left-ventricular wall: epicardium versus midmyocardium. Pflugers Arch 2005; 450: 307-16. doi: 10.1007/s00424-005-1445-z
29. Szentadrassy N, Banyasz T, Biro T, Szabo G, Toth BI, Magyar J, et al. Apico-basal inhomogeneity in distribution of ion channels in canine and human ventricular myocardium. Cardiovasc Res 2005; 65: 851-60. doi: 10.1016/j.cardiores.2004.11.022
30. Vaczi K, Hegyi B, Ruzsnavszky F, Kistamas K, Horvath B, Banyasz T, et al. 9-Anthracene carboxylic acid is more suitable than DIDS for characterization of calcium-activated chloride current during canine ventricular action potential. Naunyn Schmiedebergs Arch Pharmacol 2015; 388: 87-100. doi: 10.1007/s00210-014-1050-9
31. Kamp TJ, Hell JW. Regulation of cardiac L-type calcium channels by protein kinase A and protein kinase C. Circ Res 2000; 87: 1095-102. doi: 10.1161/01.RES.87.12.1095
32. Gomez JP, Fares N, Potreau D. Effects of Bay K 8644 on L-type calcium current from newborn rat cardiomyocytes in primary culture. J Mol Cell Cardiol 1996; 28: 2217-29. doi: 10.1006/jmcc.1996.0213
33. Szentandrassy N, Farkas V, Barandi L, Hegyi B, Ruzsnavszky F, Horvath B, et al. Role of action potential configuration and the contribution of Ca2+ and K+ currents to isoprenaline-induced changes in canine ventricular cells. Br J Pharmacol 2012; 167: 599-611. doi: 10.1111/j.1476-5381.2012.02015.x
34. Szentandrassy N, Nagy D, Ruzsnavszky F, Harmati G, Banyasz T, Magyar J, et al. Powerful technique to test selectivity of agents acting on cardiac ion channels: the action potential voltage-clamp. Curr Med Chem 2011; 18: 3737-56. doi: 10.2174/092986711796642418
35. Hiraoka M, Kawano S, Hirano Y, Furukawa T. Role of cardiac chloride currents in changes in action potential characteristics and arrhythmias. Cardiovasc Res 1998; 40: 23-33. doi: http://dx.doi.org/10.1016/S0008-6363(98)00173-4
36. Zygmunt AC, Robitelle DC, Eddlestone GT. Ito1 dictates behavior of ICl(Ca) during early repolarization of canine ventricle. Am J Physiol 1997; 273: H1096-106.
37. Harvey RD, Clark CD, Hume JR. Chloride current in mammalian cardiac myocytes. Novel mechanism for autonomic regulation of action potential duration and resting membrane potential. J Gen Physiol 1990; 95: 1077-102. doi: 10.1085/jgp.95.6.1077
38. Sorota S, Siegal MS, Hoffman BF. The isoproterenol-induced chloride current and cardiac resting potential. J Mol Cell Cardiol 1991; 23: 1191-8. doi: 10.1016/0022-2828(91)90207-3
39. Oz MC, Sorota S. Forskolin stimulates swelling-induced chloride current, not cardiac cystic fibrosis transmembrane-conductance regulator current, in human cardiac myocytes. Circ Res 1995; 76: 1063-70. doi: 10.1161/01.RES.76.6.1063
40. Tian Y, Schreiber R, Kunzelmann K. Anoctamins are a family of Ca2+-activated Cl- channels. J Cell Sci 2012; 125: 4991-8. doi: 10.1242/jcs.109553
41. Acsai K, Antoons G, Livshitz L, Rudy Y, Sipido KR. Microdomain [Ca2+] near ryanodine receptors as reported by L-type Ca2+ and Na+/Ca2+ exchange currents. J Physiol 2011; 589: 2569-83. doi: 10.1113/jphysiol.2010.202663

42. Despa S, Shui B, Bossuyt J, Lang D, Kotlikoff MI, Bers DM. Junctional cleft [Ca2+]i measurements using novel cleft-targeted Ca2+ sensors. Circ Res 2014; 115: 339-47. doi: 10.1161/CIRCRESAHA.115.303582
43. Yang T, Colecraft HM. Calmodulin regulation of TMEM16A and 16B Ca(2+)-activated chloride channels. Channels (Austin). 2016; 10: 38-44. doi: 10.1080/19336950.2015.1058455
44. Fink M, Noble PJ, Noble D. Ca2+-induced delayed afterdepolarizations are triggered by dyadic subspace Ca2+ affirming that increasing SERCA reduces aftercontractions. Am J Physiol Heart Circ Physiol. 2011; 301: H921-35. doi: 10.1152/ajpheart.01055.2010
45. Horvath B, Banyasz T, Jian Z, Hegyi B, Kistamas K, Nanasi PP, et al. Dynamics of the late Na+ current during cardiac action potential and its contribution to afterdepolarizations. J Mol Cell Cardiol 2013; 64: 59-68. doi: 10.1016/j.yjmcc.2013.08.010
46. Verkerk AO, Veldkamp MW, Bouman LN, van Ginneken AC. Calcium-activated Cl(-) current contributes to delayed afterdepolarizations in single Purkinje and ventricular myocytes. Circulation. 2000; 101: 2639-44. doi: doi:10.1161/01.CIR.101.22.2639
47. Hennessey JA, Boczek NJ, Jiang YH, Miller JD, Patrick W, Pfeiffer R, et al. A CACNA1C variant associated with reduced voltage-dependent inactivation, increased CaV1.2 channel window current, and arrhythmogenesis. PLoS One. 2014; 9: e106982. doi: 10.1371/journal.pone.0106982
48. Boczek NJ, Miller EM, Ye D, Nesterenko VV, Tester DJ, Antzelevitch C, et al. Novel Timothy syndrome mutation leading to increase in CACNA1C window current. Heart Rhythm. 2015; 12: 211-9. doi: 10.1016/j.hrthm.2014.09.051
49. Banyasz T, Horvath B, Jian Z, Izu LT, Chen-Izu Y. Profile of L-type Ca(2+) current and Na(+)/Ca(2+) exchange current during cardiac action potential in ventricular myocytes. Heart Rhythm 2012; 9: 134-42. doi: 10.1016/j.hrthm.2011.08.029.
50. Boyden PA. Chasing calcium. Heart Rhythm. 2012; 9: 143-4. doi: 10.1016/j.hrthm.2011.09.057
51. Saleh SN, Greenwood IA. Activation of chloride currents in murine portal vein smooth muscle cells by membrane depolarization involves intracellular calcium release. Am J Physiol Cell Physiol 2005; 288: C122-31. doi: 10.1152/ajpcell.00384.2004
52. Nagy N, Szuts V, Horváth Z, Seprényi G, Farkas AS, Acsai K, et al. Does small-conductance calcium-activated potassium channel contribute to cardiac repolarization? J Mol Cell Cardiol 2009; 47: 656-63. doi: 10.1016/j.yjmcc.2009.07.019.
53. Weber CR, Piacentino V 3rd, Ginsburg KS, Houser SR, Bers DM. Na(+)-Ca(2+) exchange current and submembrane [Ca(2+)] during the cardiac action potential. Circ Res 2002; 90: 182-9. doi:10.1161/hh0202.103940
54. Janvier NC, Harrison SM, Boyett MR. The role of inward Na(+)-Ca2+ exchange current in the ferret ventricular action potential. J Physiol 1997; 498: 611-25. doi: 10.1113/jphysiol.1997.sp021887
55. Kistamas K, Szentandrassy N, Hegyi B, Vaczi K, Ruzsnavszky F, Horvath B, et al. Changes in intracellular calcium concentration influence beat-to-beat variability of action potential duration in canine ventricular myocytes. J Physiol Pharmacol 2015; 66: 73-81.
56. Scriven DR, Dan P, Moore ED. Distribution of proteins implicated in excitation-contraction coupling in rat ventricular myocytes. Biophys J 2000; 79: 2682-91. doi: 10.1016/S0006-3495(00)76506-4
57. Shang W, Lu F, Sun T, Xu J, Li LL, Wang Y, et al. Imaging Ca2+ nanosparks in heart with a new targeted biosensor. Circ Res 2014; 114: 412-20. doi: 10.1161/CIRCRESAHA.114.302938
58. Bao R, Lifshitz LM, Tuft RA, Bellve K, Fogarty KE, ZhuGe R. A close association of RyRs with highly dense clusters of Ca2+-activated Cl- channels underlies the activation of STICs by Ca2+ sparks in mouse airway smooth muscle. J Gen Physiol 2008; 132: 145-60. doi: 10.1085/jgp.200709933
59. Pasek M, Simurda J, Orchard CH. Effect of Ca2+ efflux pathway distribution and exogenous Ca2+ buffers on intracellular Ca2+ dynamics in the rat ventricular myocyte: a simulation study. Biomed Res Int 2014; 2014: 920208. doi: 10.1155/2014/920208
60. Berkefeld H, Sailer CA, Bildl W, Rohde V, Thumfart JO, Eble S, et al. BKCa-Cav channel complexes mediate rapid and localized Ca2+-activated K+ signaling. Science 2006; 314: 615-20. doi: 10.1126/science.1132915
61. O'Driscoll KE, Leblanc N, Hatton WJ, Britton FC. Functional properties of murine bestrophin 1 channel. Biochem Biophys Res Commun 2009; 384: 476-81. doi: 10.1016/j.bbrc.2009.05.008

62. O'Driscoll KE, Hatton WJ, Burkin HR, Leblanc N, Britton FC. Expression, localization, and functional properties of Bestrophin 3 channel isolated from mouse heart. Am J Physiol Cell Physiol 2008; 295: C1610-24. doi: 10.1152/ajpcell.00461.2008
63. Perino A, Ghigo A, Scott JD, Hirsch E. Anchoring proteins as regulators of signaling pathways. Circ Res 2012; 111: 482-92. doi: 10.1161/CIRCRESAHA.111.262899.
64. Huang WC, Xiao S, Huang F, Harfe BD, Jan YN, Jan LY. Calcium-activated chloride channels (CaCCs) regulate action potential and synaptic response in hippocampal neurons. Neuron 2012; 74: 179-92. doi: 10.1016/j.neuron.2012.01.033.
65. Dam VS, Boedtkjer DM, Aalkjaer C, Matchkov V. The bestrophin- and TMEM16A-associated Ca2+- activated Cl- channels in vascular smooth muscles. Channels (Austin) 2014; 8: 361-9. doi: 10.4161/chan.29531
66. Dam VS, Boedtkjer DM, Nyvad J, Aalkjaer C, Matchkov V. TMEM16A knockdown abrogates two different Ca2+-activated Cl- currents and contractility of smooth muscle in rat mesenteric small arteries. Pflugers Arch 2014; 466: 1391-409. doi: 10.1007/s00424-013-1382-1
67. Bharill S, Fu Z, Palty R, Isacoff EY. Stoichiometry and specific assembly of Best ion channels. Proc Natl Acad Sci U S A 2014; 111: 6491-6. doi: 10.1073/pnas.1400248111
68. Tien J, Lee HY, Minor DL, Jr., Jan YN, Jan LY. Identification of a dimerization domain in the TMEM16A calcium-activated chloride channel (CaCC). Proc Natl Acad Sci U S A 2013; 110: 6352-7. doi: 10.1073/pnas.1303672110
69. Hong TT, Smyth JW, Gao D, Chu KY, Vogan JM, Fong TS, et al. BIN1 localizes the L-type calcium channel to cardiac T-tubules. PLoS Biol 2010; 8: e1000312. doi: 10.1371/journal.pbio.1000312
70. Chen-Izu Y, McCulle SL, Ward CW, Soeller C, Allen BM, Rabang C, et al. Three-dimensional distribution of ryanodine receptor clusters in cardiac myocytes. Biophys J 2006; 91: 1-13. doi: 10.1529/biophysj.105.077180

Figures with Figure Legends

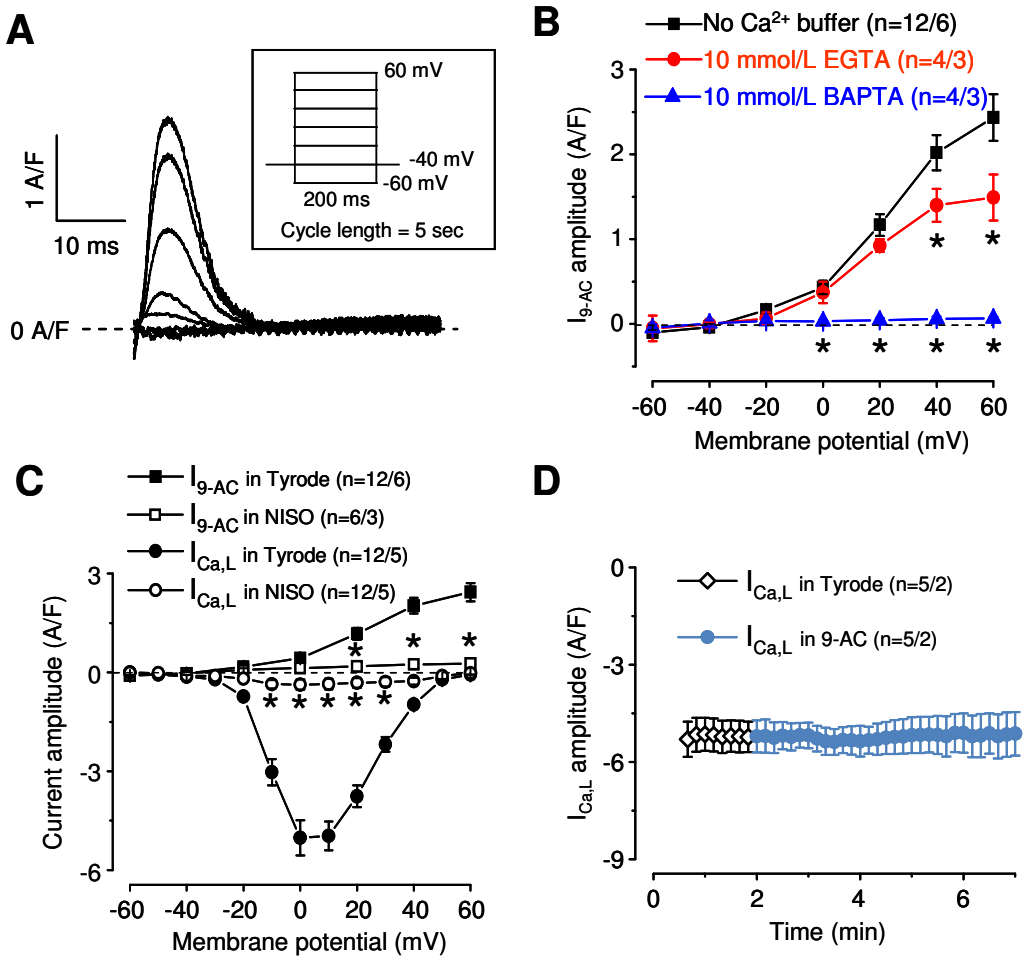

Fig. 1. Ca^{2+}- and voltage-dependence of $I_{Cl(Ca)}$ in canine ventricular myocytes.
(A) Representative $I_{Cl(Ca)}$ traces, determined as 0.5 mmol/L 9-AC-sensitive current ($I_{9\text{-}AC}$), at test potentials ranging from −60 to +60 mV without applying a Ca^{2+} buffer in the pipette (voltage protocol shown in the inset). (B) $I_{9\text{-}AC}$ amplitudes plotted as a function of the test potential under various intracellular Ca^{2+}-buffering conditions: without Ca^{2+} buffer, 10 mmol/L EGTA or 10 mmol/L BAPTA in the pipette solution). (C) Voltage-dependence of $I_{9\text{-}AC}$ and $I_{Ca,L}$ measured without Ca^{2+} buffer in control (in Tyrode) and in the presence of 1 µmol/L nisoldipine (in NISO). (D) $I_{Ca,L}$ amplitude measured in the absence (open diamonds) and presence of 0.5 mmol/L 9-AC (filled circles). Symbols, columns and bars represent mean ± SEM values. Asterisks denote significant difference from control, n indicates the number of experiments (number of cells / number of hearts).

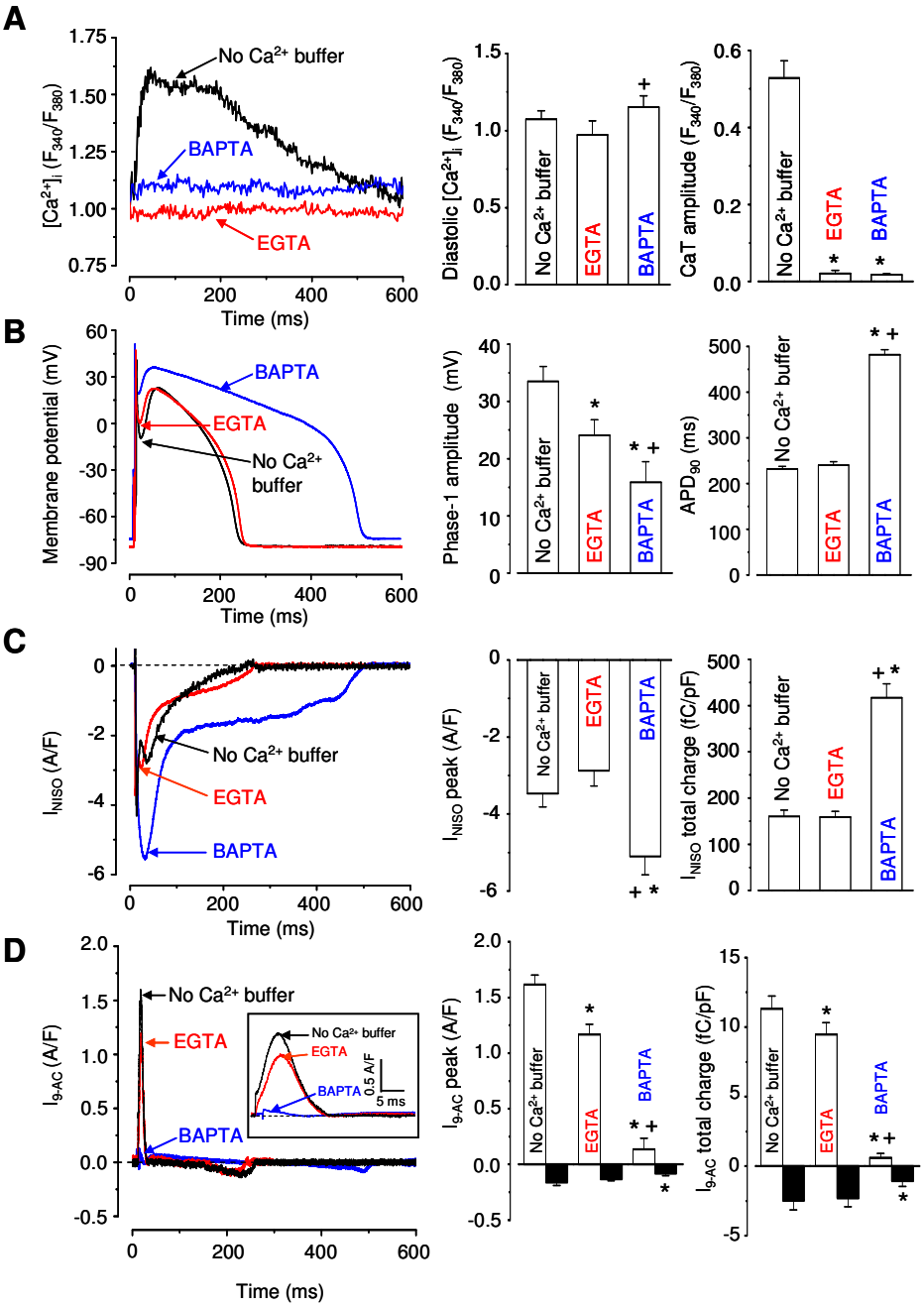

Fig. 2. Effect of various intracellular buffering conditions on the simultaneously recorded cardiac AP, intracellular Ca^{2+} transient (CaT), I_{NISO}, and $I_{9\text{-}AC}$.
Cells were voltage-clamped through pipettes containing no Ca^{2+} buffer (n=4/2, where number of cells / number of hearts is given), 10 mmol/L EGTA (n=9/4) or 10 mmol/L BAPTA (n=6/3). (A) Representative CaTs (average of ten traces, measured with Fura-2-AM), diastolic $[Ca^{2+}]_i$, and CaT amplitude. (B) Superimposed representative APs, phase-1 amplitudes, and action potential duration (APD_{90}). (C) Representative I_{NISO} traces (1 µmol/L nisoldipine-sensitive current), I_{NISO} peak and total charge. (D) APVC recordings of $I_{Cl(Ca)}$ (0.5 mmol/L 9-AC-sensitive current), $I_{9\text{-}AC}$ peak densities and total charges carried by outward (white columns) and inward currents (black columns). The first 35 ms of the representative traces is displayed enlarged in the inset. Columns and bars indicate mean ± SEM values, asterisks denote significant differences from unbuffered condition, + symbols indicate significant differences between the effects of EGTA and BAPTA.

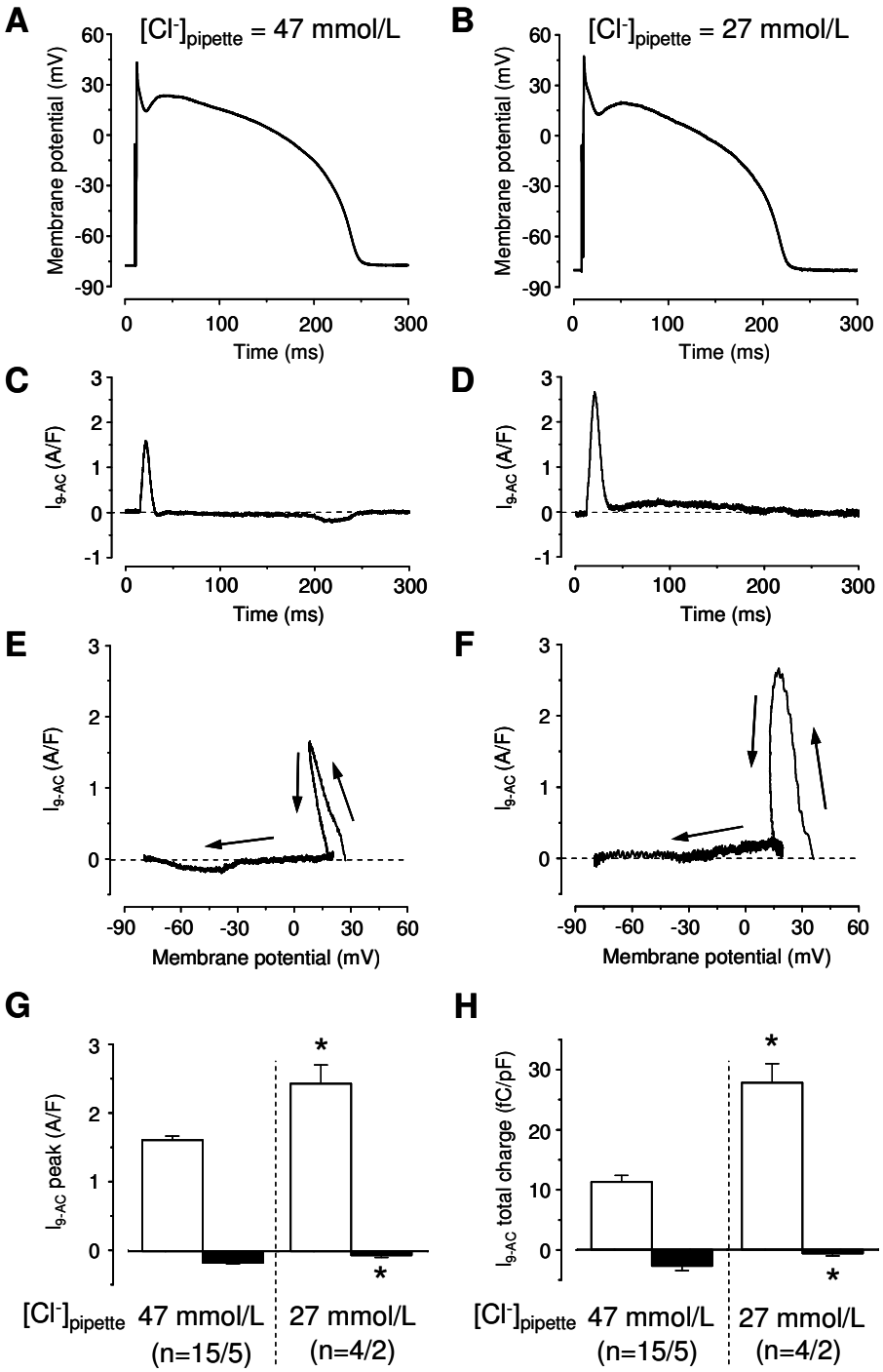

Fig. 3. Influence of $[Cl^-]_i$ on $I_{Cl(Ca)}$ profile during self AP voltage-clamp recordings.
The pipette solution contained either 47 mmol/L (A, C, E) or 27 mmol/L Cl^- (B, D, F). Representative APs (A, B) and the corresponding APVC recordings of $I_{9\text{-}AC}$ (C, D) are displayed. Panels E and F show phase-plane trajectories generated by plotting $I_{9\text{-}AC}$ amplitudes against the corresponding values of membrane potential. Arrows indicate the temporal sequence. $I_{9\text{-}AC}$ peak densities (G) and total charges (H) estimated for outward (white columns) and inward currents (black columns). Columns and bars indicate mean ± SEM values, asterisks denote significant differences from data obtained with 47 mmol/L Cl^- containing pipettes. n indicates the number of experiments where number of cells / number of hearts is given.

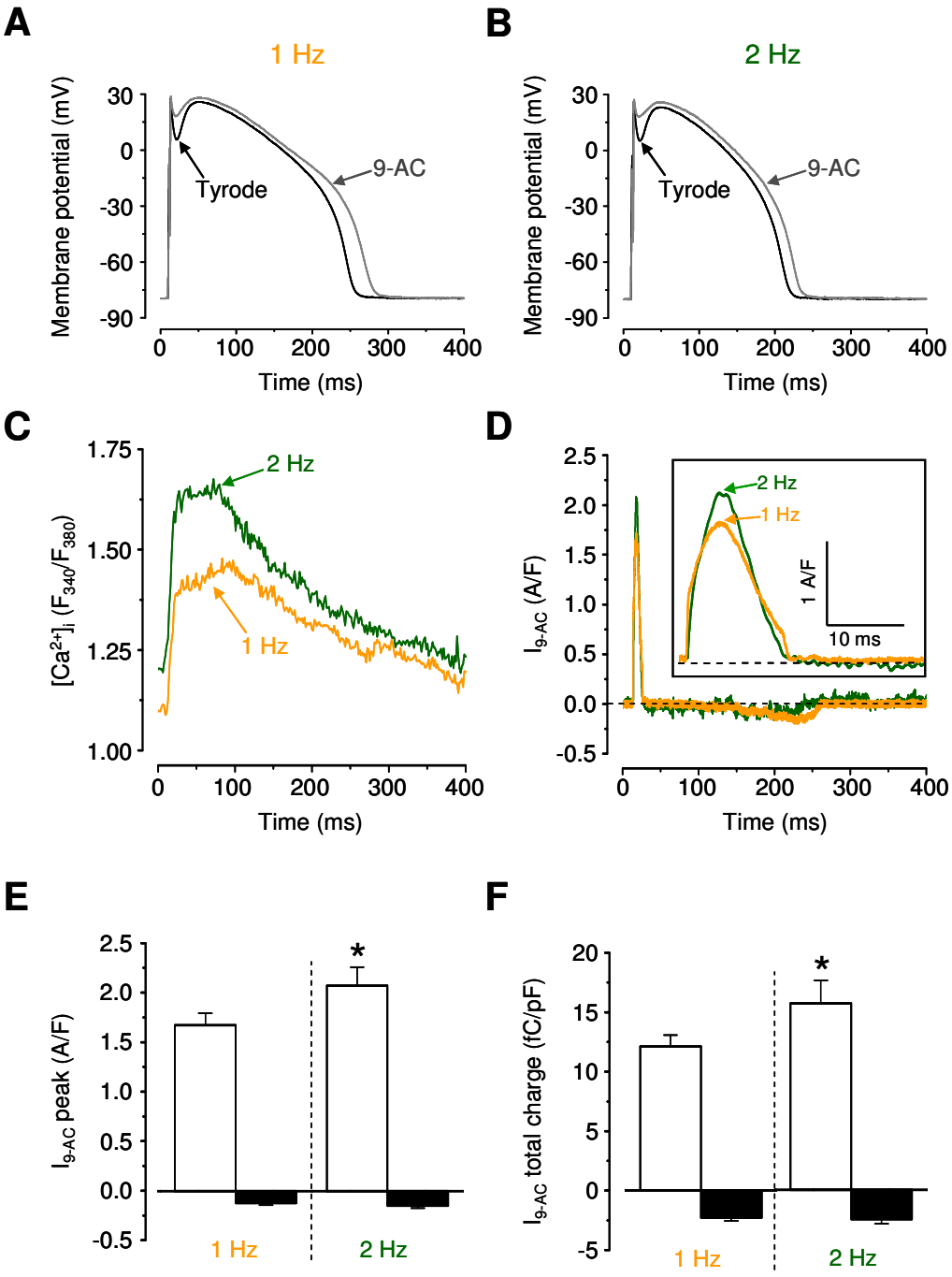

Fig. 4. Rate-dependence of $I_{Cl(Ca)}$ under APVC conditions.
Upper panels show representative APs in control and in 0.5 mmol/L 9-AC at 1 (A) and 2 Hz (B) stimulatory frequencies. Representative Ca^{2+} transients (C) and $I_{9\text{-}AC}$ traces (D) recorded at these pacing rates. $I_{9\text{-}AC}$ peak densities (E) and total charges (F) measured during outward (white columns) and inward currents (black columns). The first 30 ms of the current traces is shown enlarged in the inset of panel D. Columns and bars indicate mean ± SEM values, asterisks denote significant differences from data obtained at 1 Hz. Number of experiments at both frequencies were 5 cells / 3 hearts.

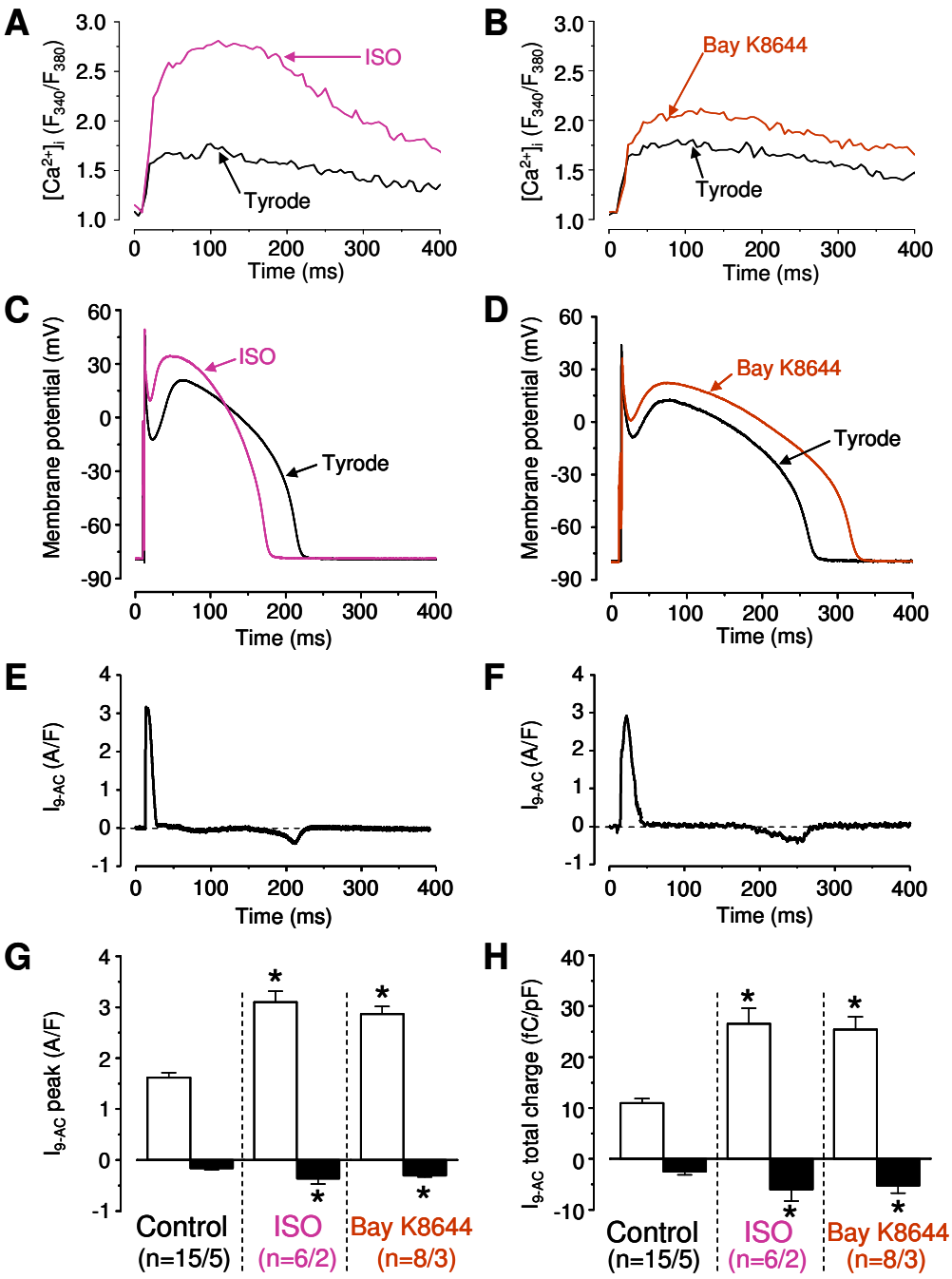

Fig. 5. Stimulation of $I_{Cl(Ca)}$ by isoproterenol and Bay K8644.
Representative traces of Ca^{2+} transients (A, B) and APs (C, D) in control and in the presence of either 10 nmol/L isoproterenol (ISO, A and C) or 20 nmol/L Bay K8644 (B and D). Representative $I_{Cl(Ca)}$ records, dissected by 0.5 mmol/L 9-AC using the AP recorded in Tyrode solution as the command signal, in the presence of ISO (E) and Bay K8644 (F). $I_{9\text{-}AC}$ peak densities (G) and total charges (H) estimated for outward (white columns) and inward currents (black columns). Columns and bars indicate mean ± SEM values, asterisks denote significant differences from control. n indicates the number of experiments where number of cells / number of hearts is given.

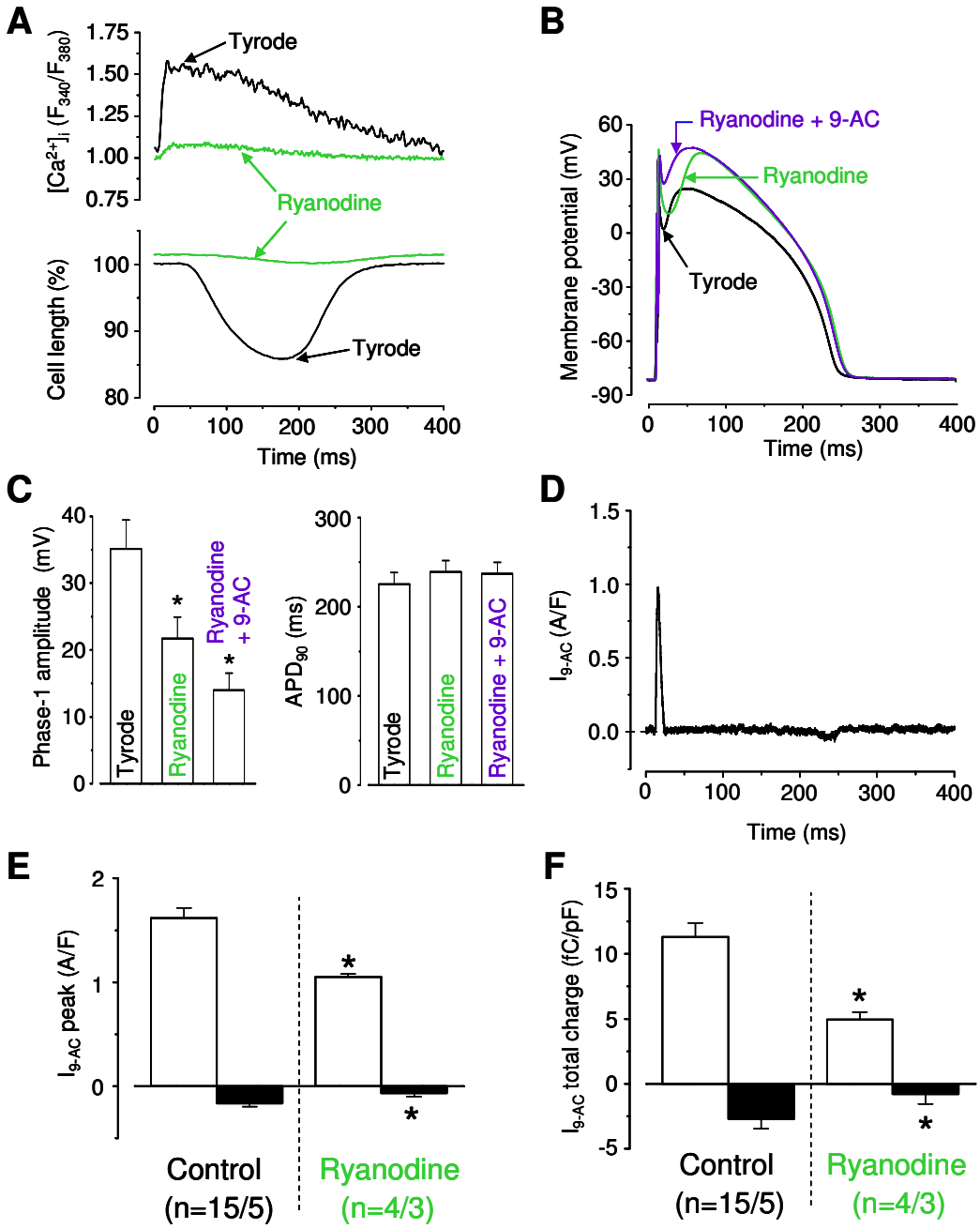

Fig. 6. Role of SR Ca^{2+}-release in $I_{Cl(Ca)}$ activation.
(A) Effects of ryanodine on Ca^{2+} transient (top) and cell shortening (bottom) in a field-stimulated myocyte. (B) Representative traces of APs recorded in Tyrode solution (control), in the presence of 10 µmol/L ryanodine and following an additional superfusion with 0.5 mmol/L 9-AC. (C) Average phase-1 amplitudes and APD_{90} values obtained under the above conditions in 4 myocytes of 3 animals. (D) Representative $I_{Cl(Ca)}$ record measured in the presence of ryanodine with APVC. $I_{Cl(Ca)}$ was dissected by 0.5 mmol/L 9-AC ($I_{9\text{-}AC}$) using the AP recorded in Tyrode solution as the command signal. E and F panels show average results on $I_{9\text{-}AC}$ peak densities and total charges flowing during the outward (white columns) and inward (black columns) current components. Columns and bars indicate mean ± SEM values, asterisks denote significant differences from control. n indicates the number of experiments where number of cells / number of hearts is given.

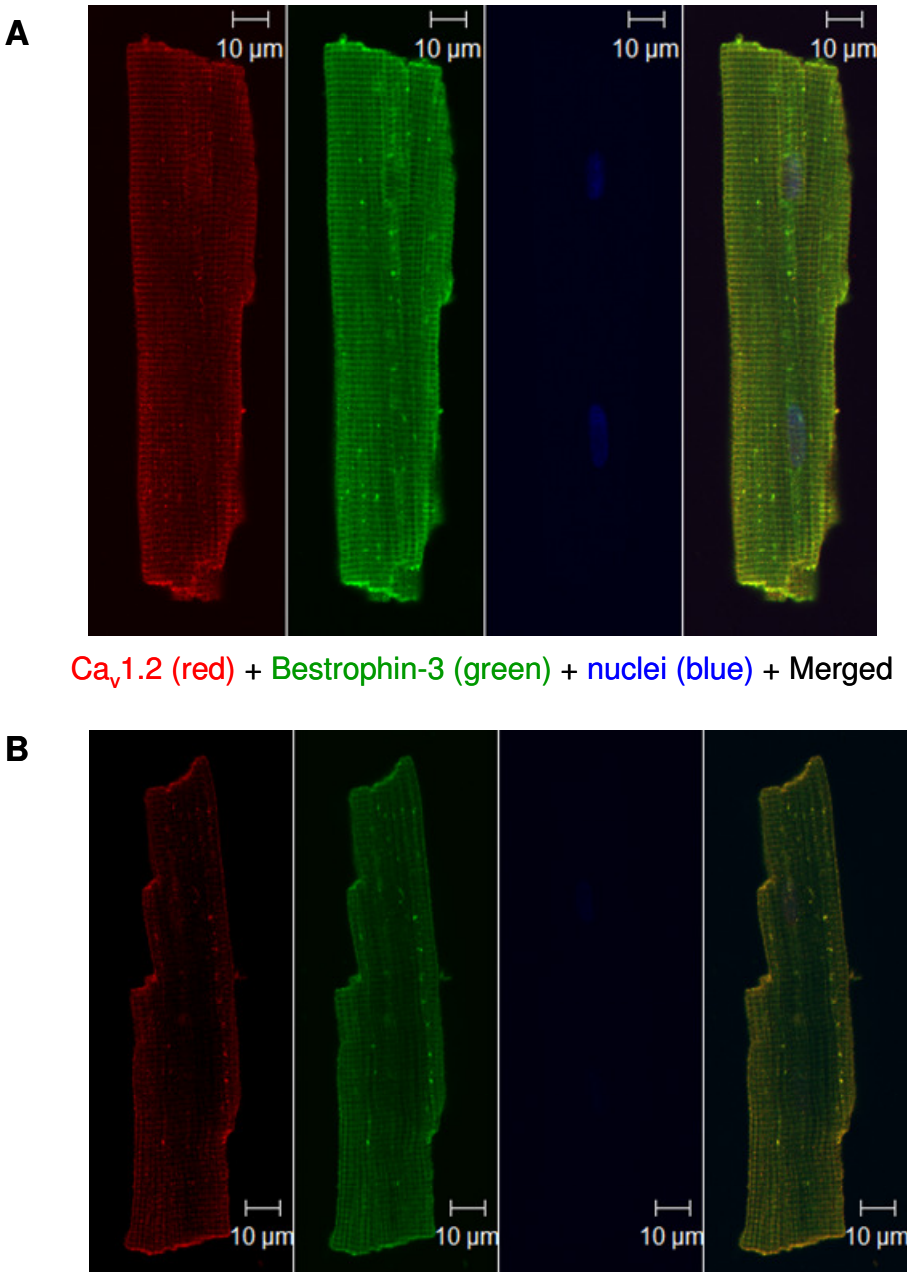

Fig. 7. Confocal images showing the expression pattern of $Ca_v1.2$, TMEM16A, and Bestrophin-3 in canine ventricular myocytes.
(A) Representative cell showing the expression of $Ca_v1.2$, Bestrophin-3, and nuclear staining in red, green, and blue, respectively, from left to right. The far right panel represents the overlay of the three images.
(B) Representative cell showing the expression of TMEM16A, Bestrophin-3, and nuclear staining in red, green, and blue, respectively, from left to right. The far right panel represents the overlay of the three images.

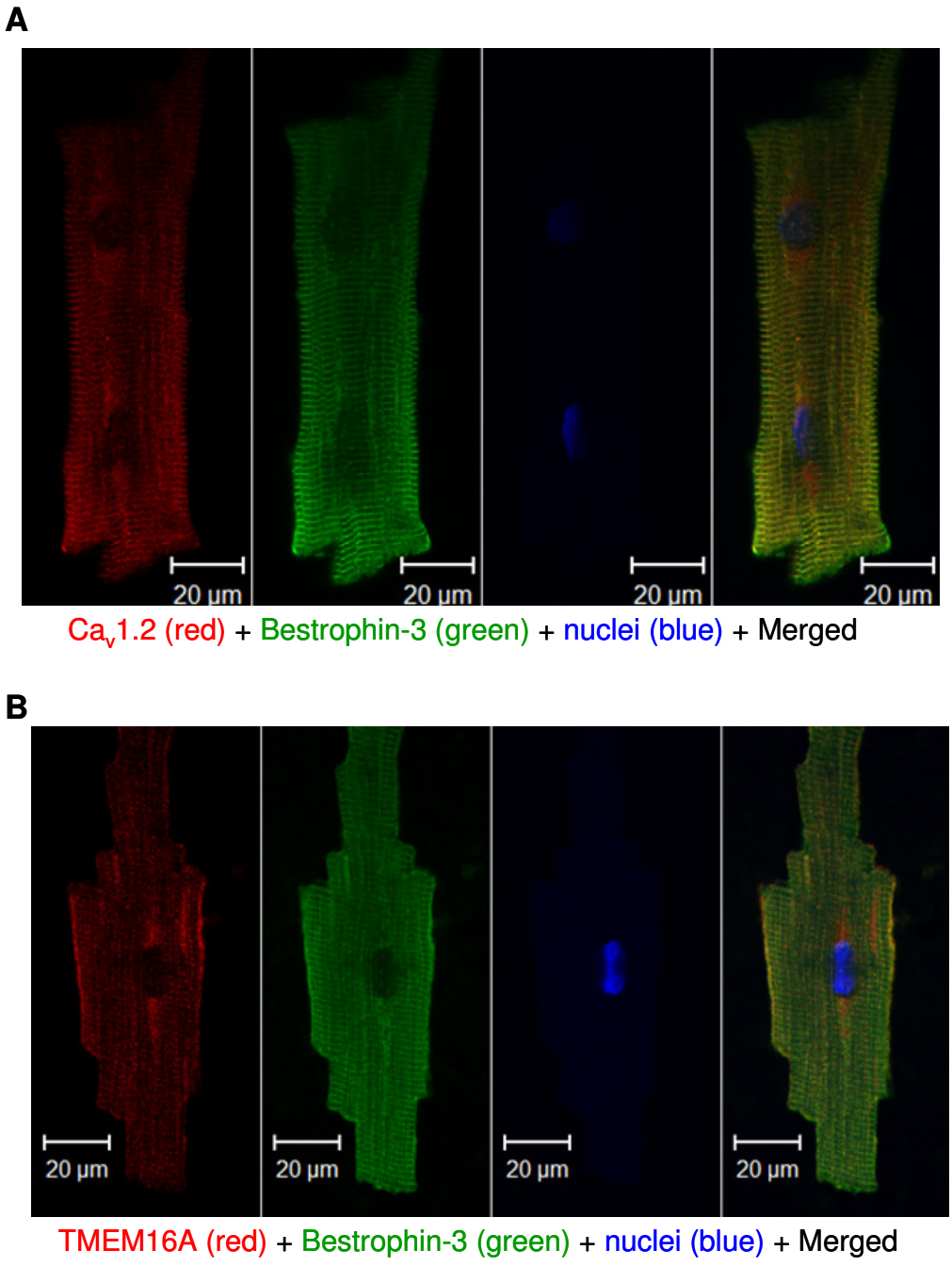

Fig. 8. Confocal images showing the expression pattern of $Ca_v1.2$, TMEM16A, and Bestrophin-3 in left ventricular myocytes obtained from non-diseased human hearts.
(A) Representative cell showing the expression of $Ca_v1.2$, Bestrophin-3, and nuclear staining in red, green, and blue, respectively, from left to right. The far right panel represents the overlay of the three images.
(B) Representative cell showing the expression of TMEM16A, Bestrophin-3, and nuclear staining in red, green, and blue, respectively, from left to right. The far right panel represents the overlay of the three images.

Online Supplement

Detailed Methods

All reagents were dissolved in DMSO or 96 % ethanol. Equivalent volumes of solvents did not affect any of the physiological parameters studied. The osmolarity of all extracellular solutions were carefully adjusted to 295 ± 3 mmol/kg with a vapor pressure osmometer (Vapro 5520, Wescor Inc., Logan, UT, USA).

Isolation of canine left ventricular myocytes

Cell isolation was carried out by enzymatic dispersion using the segment perfusion technique described previously [1]. Adult healthy beagle dogs of both sexes were anesthetized by intramuscular application of a mixture of 10 mg/kg ketamine hydrochloride (Calypsol, Richter Gedeon, Budapest, Hungary) and 1 mg/kg xylazine hydrochloride (Sedaxylan, Eurovet Animal Health BV, Bladel, The Netherlands). After achieving complete narcosis, the chest was opened, the heart was quickly removed and washed in cold Tyrode solution containing (in mmol/L): NaCl 144, KCl 5.6, $CaCl_2$ 2.5, $MgCl_2$ 1.2, 4-(2-Hydroxyethyl)piperazine-1-ethanesulfonic acid (HEPES) 5, glucose 10 (pH = 7.4; adjusted with NaOH). The left anterior descending coronary artery was cannulated and perfused with a nominally Ca^{2+}-free JMM solution (Minimum Essential Medium Eagle, Joklik Modification, product no. M0518) supplemented with the followings: 2.5 g/L taurine, 200 mg/L NaH_2PO_4, 1.4 g/L $NaHCO_3$, 175 mg/L pyruvic acid, 13.5 mg/L allopurinol, and 750 mg/L D-ribose, having pH of 6.8. JMM solution was gassed with a mixture of 95 % O_2 and 5 % CO_2. Then a wedge-shaped section of the left ventricular wall supplied by the left anterior descending coronary artery was dissected. Following further 5 min of perfusion to completely remove blood from the tissue, 0.9 g/L collagenase (type II, 245 U/mg; Worthington Biochemical Co., Lakewood, NJ, USA), 2 g/L bovine serum albumin (Fraction V.), and 50 µmol/L $CaCl_2$ were added to the JMM solution. Enzymatic digestion took usually 25-35 minutes which was followed by the collection of isolated cells. During the enzymatic digestion the solution was kept at 37 ºC. The tissue was cut with a scalpel and the middle portion of the free left ventricular wall containing mainly midmyocardial cells was cut into pieces, sedimented and filtered four times to remove big chunks. During this procedure Ca^{2+} concentration of the JMM solution was gradually restored to the final value of 1.8 mmol/L. Finally, cells were placed into MEM solution (Minimum Essential Medium Eagle, product no. M0643) supplemented with the followings: 2.5 g/L taurine, 200 mg/L NaH_2PO_4, 2.2 g/L $NaHCO_3$, 175 mg/L pyruvic acid, 13.5 mg/L allopurinol, 750 mg/L D-ribose (pH = 7.3, achieved by bubbling the solution with a mixture of 95 % O_2 and 5 % CO_2) and stored at 15 ºC until use. The percentage of living cells, showing clear cytoplasm and striations with sharp edges, was typically 30-60 %.

Isolation of left ventricular myocytes from non-diseased human donor hearts

Cell isolation was carried out by enzymatic dispersion as described previously [2].

Electrophysiology

Cells were placed in a 1 mL volume plexiglass chamber and continuously superfused with Tyrode solution supplied by a gravity driven system at a speed of 2 mL/min. During experiments the bath temperature was set to 37 ºC by a temperature controller (Cell MicroControls, Norfolk, VA, USA). The cells were visualized by an inverted microscope (Eclipse TE2000-U, Nikon, Japan) placed in a Faraday cage on an anti-vibration table. Electrical signals were recorded with intracellular amplifiers (MultiClamp 700A or 700B, Molecular Devices, Sunnyvale, CA, USA) and recorded with pClamp 10 software (Molecular Devices) after analogue-digital conversion (Digidata 1440A or 1332, Molecular Devices). Electrodes were fabricated from borosilicate glass having tip resistances of 2-3 MΩ after filling with pipette solution. Membrane currents were recorded using the whole-cell configuration of the patch-clamp technique. After establishing high (1-10 GΩ) resistance seal by gentle suction, the cell membrane beneath the tip of the electrode was disrupted by further suction or by applying 1.5 V electrical pulses for 1 ms. The series resistance was typically 4-6 MΩ. Experiments were discarded when the series resistance was high or substantially increased during the measurement. To preserve the normal Ca^{2+} homeostasis, we used internal solution containing (in mmol/L): K-aspartate 110, KCl 45, K_2-ATP 3, $MgCl_2$ 1, HEPES 5, pH = 7.2 (adjusted using KOH). To examine the influence of the Cl^-

concentration on $I_{Cl(Ca)}$, 20 mmol/L of KCl was replaced by the same amount of K-Aspartate. In experiments aimed to eliminate $[Ca^{2+}]_i$ transients during the AP, 10 mmol/L EGTA or 10 mmol/L BAPTA were used in the pipette (without adding any Ca^{2+}), and the concentration of K-Aspartate was compensatory reduced in both cases. To buffer intracellular free Ca^{2+} to 1.1 µmol/L [3] we used the internal solution containing (in mmol/L): K-Aspartate 107, KCl 38, K_2-ATP 3, $MgCl_2$ 1, HEPES 5, BAPTA 4.5, $CaCl_2$ 3.5 (pH = 7.2). In case of $I_{Ca,L}$ measurement, 3 mmol/L 4-aminopyridine was added to the Tyrode solution and the internal solution contained (in mmol/L) KCl 110, KOH 40, HEPES 10, EGTA 10, tetraethylammonium chloride 20, K_2-ATP 3 (pH = 7.2 with KOH). The osmolarity of all internal solutions was between 284 and 288 mmol/kg.

$I_{Cl(Ca)}$ was defined as a 9-AC-sensitive current ($I_{9\text{-}AC}$) obtained by pharmacological subtraction [1]. In conventional voltage-clamp measurements, $I_{Cl(Ca)}$ was determined within the voltage range of −60 to +60 mV using 200 ms long voltage pulses arising from the holding potential of −40 mV and applied at a rate of 0.2 Hz. Current–voltage relations for $I_{Ca,L}$ were obtained by applying a series of 400-ms-long test pulses at 0.2 Hz increasing up to +60 mV in 10 mV steps from the holding potential of −40 mV. Current amplitudes were calculated as differences between peak and pedestal values.

During APVC experiments Sequential Dissection experiments were conducted according to the method described previously [4, 5]. Action potentials were recorded in whole-cell configuration of current-clamp mode from the myocytes superfused with Tyrode solution. The pipette solution was identical to that used for the normal Ca^{2+} homeostasis condition (see above). Cells were continuously paced through the patch-pipette with supra-threshold depolarizing pulses of 1-2 ms duration delivered at steady stimulation frequency of 1 Hz (except when 2 Hz stimulation was used on Fig. 4.) so as a 1-2 ms gap between the stimulus artifact and the upstroke of the AP could occur. Ten subsequent APs were recorded and immediately analyzed from each cell. One of these APs, recorded always in pure Tyrode solution, having duration (and overall shape) closest to the average, was delivered to the same cell at the identical frequency as command voltage after switching the amplifier to voltage-clamp mode. The current trace obtained under these conditions (I_{base}) is a horizontal line positioned at the zero level except for the very short segment corresponding to the action potential upstroke. To isolate the 1st current of interest, its blocker was used to reveal it from the net membrane current (I_{drug1}). The profile of this current was determined by subtracting the post-drug curve from the pre-drug one ($I_1 = I_{base} - I_{drug1}$). It was followed by the isolation of the 2nd current of interest by applying the specific modulator of the 2nd current in the continuous presence of the first drug, and then the 2nd current was obtained by subtraction ($I_2 = I_{drug1} - I_{drug1+drug2}$). These currents were always recorded after the action of the applied agent reached steady-state. The following agents were used for dissecting the currents: 0.5 mmol/L 9-AC for $I_{9\text{-}AC}$, basically $I_{Cl(Ca)}$, 1 µmol/L nisoldipine for I_{NISO}, consisting of $I_{Ca,L}$ and the ion current flowing through Na^+/Ca^{2+} exchanger as the two most important component. The following currents were studied and defined in APVC experiments as:

$I_{9\text{-}AC}$ = I (measured prior to the application of 9-AC) – I (measured in the presence of 9-AC),

I_{NISO} = I (measured in the presence of 9-AC) – I (measured in the presence of NISO+9-AC).

Ion currents were normalized to cell capacitance, determined in each cell using hyperpolarizations from +10 to −10 mV for 15 ms. Cell capacitance was 129±6 pF in the average of the 85 myocytes studied.

Measurement of intracellular Ca^{2+} concentration ($[Ca^{2+}]_i$)

Myocytes were loaded in Tyrode solution with the membrane-permeant form of 5 µmol/L Fura-2 in the presence of Pluronic F-127 for 30 min at room temperature. A period of minimum 30 min was allowed for de-esterification of the dye at room temperature then cells were stored at 15 ºC until the experiment. Loaded cells were illuminated using a 40x oil immersion objective (CFI S-Fluor 40x oil, Nikon) or 40 x air objective (40UV/340, Olympus). Cells were excited with 340 and 380 nm light from a xenon arc lamp (Ushio Deutschland GmbH, Steinhöring, Germany). Excitatory wavelengths were altered by a dual-wavelength excitation monochromator and an on-line connected microcomputer (DeltaScan, Photon Technology International, New Brunswick, NJ, USA). Fluorescence emission was monitored at 510 nm using a R1527P photomultiplier tube (Hamamatsu Photonics Deutschland GmbH., Herrsching am Ammersee, Germany) at an acquisition rate of 200 Hz. Changes in intracellular free Ca^{2+} levels were approximated by the ratio of the fluorescence intensity obtained at

340 and 380 nm excitation after correction for nonspecific background fluorescence and recorded using FeliX32 Software & BryteBox Interface (Photon Technology International, New Brunswick, NJ, USA) and presented as F_{340}/F_{380} on Figures. Ten consecutive $[Ca^{2+}]_i$ transients were averaged and analyzed off-line.

Single cell shortening measurements

Myocyte contractions were recorded with a video-edge detector system (VED-105, Crescent Electronics, Sandy, Utah, USA) sampling at 240 Hz. Shortening of isolated cardiomyocytes was expressed as a percentage of diastolic cell length measured in control. The analogue signal of cell length was amplified (DC amplifier, Főnixcomp Ltd, Hungary), digitized (Digidata 1440A, Molecular Devices) and recorded using pClamp 10 software (Molecular Devices). During subsequent off-line analysis, 10 consecutive curves were averaged.

Immunolabeling, confocal imaging and Western blotting

Canine left ventricular myocytes were seeded into glass coverslips and kept at 37 °C for 2-3 hours. Living cells attached to the surface of the coverslips. Human left ventricular samples were embedded in Cryomatrix (Thermo Scientific, Rockford, IL, USA) and 10 µm thick sections were cut at −20°C using Shandon Cryotome E (Thermo Electron Corporation, Waltham, MA, USA). Sections were let to dry and the appropriate immunohistochemistry was performed. Immunolabeling was started with paraformaldehyde fixation (4 %, 15 min, 22 °C) of either isolated myocytes seeded into the glass coverslips or the frozen tissue sections. Following three times repeated washing (10 min, Phosphate Buffered Saline (PBS) or PBS-Tween20 containing 100 mmol/L glycine as a quenching agent), cells and tissue samples were permeabilized with Triton-X-100 (0.1 v/v%, 10 min, 22 °C) and then blocked with 1 or 4% BSA solution (30 min or 60 min, 22 °C, respectively). Cells were then probed with anti-TMEM16A (Santa Cruz Biotechnology, Dallas, TX, USA, sc-135235; rabbit, 1:200), anti-Bestrophin-3 (Santa Cruz Biotechnology, Dallas, TX, USA, sc-70147, goat, 1:200), anti-$Ca_v1.2$ (Santa Cruz Biotechnology, Dallas, TX, USA, sc-16229R, rabbit, 1:200), anti-ryanodine receptor (BD Biosciences, San Jose, CA, USA; mouse, 1:200), or with anti-cytochrome c (Santa Cruz Biotechnology, mouse, 1:200) primary antibodies. These primary antibodies were used overnight in 1 % BSA solution at 4 °C. Isolated human cells were placed on glass microscope slides and fixed with ice cold acetone for 5 minutes. Cells were rehydrated using 5% BSA solution for 2-3 hours and then washed with PBS (three times for 15 min at room temperature). In the case of isolated human cells and cryosections of human left ventricular tissues primary antibodies against TMEM16A, Bestrophin-3 and Cav1.2 protein were used in 1:100 dilution (in 1% BSA, 4°C, overnight). The procedure was continued with the appropriate secondary antibody labeling as follows: biotinylated anti-rabbit, anti-mouse or anti-goat antibody (Vector Laboratories, Burlingame, CA, USA, 1:300, 45 min, 22 °C) then Streptavidine Alexa488 (Life Technologies, Carlsbad, CA, USA; 1:100, 30 min, 22 °C) incubation and finally with Cy3 anti-mouse or anti-rabbit labeling (Vector Labs; 1:500, 60 min, 22 °C). The specific staining was tested by omitting the primary antibodies during the incubation procedure and also by Western blotting (see details below) and immunocytochemistry (Supplementary Fig. 2). To visualize the nuclei, cells were mounted with Vectashield mounting medium containing 4',6-diamidino-2-phenylindole (DAPI, Vector Labs.). Images were taken using Zeiss laser scanning confocal microscope (Zeiss LSM 510 Meta; using 488, 543 and 405 nm excitation wavelengths and 40x oil immersion objective).

The Pearson correlation coefficient was used to quantify the degree of co-localization between fluorophores. A correlation between the intensities could reflect a direct or indirect molecular interaction. All analysis and image processing was performed using Zeiss LSM510 Software.

Total cell lysates isolated from canine left ventricular cardiomyocytes were prepared and used for Western blot experiments. Samples were subjected to SDS-PAGE (7.5 % gels loaded with 40 µg protein per lane) and transferred to nitrocellulose membranes (Bio-Rad). The nitrocellulose-bound proteins were then blocked with 5 % dry milk in phosphate-buffered saline (PBS; pH 7.4) and probed with anti-TMEM16A primary antibodies followed by the appropriate HRP-conjugated secondary antibody labeling. The immunoreactive bands were visualised using an enhanced chemiluminescence Western blotting Pico or Femto detection kit (Thermo Scientific, Rockford, IL, USA) in a Fujifilm Labs-3000 dark box.

Specificity of the used antibodies

TMEM16A

To test the specificity of anti-TMEM16A antibody we performed Western blot experiments on canine left ventricular myocytes and human left ventricular tissue samples. In all cases a strong and solid single band could be detected (Supplementary Fig. 2A). The molecular weight however was lower than the predicted 114 kDa appearing consistently between 70 and 110 kDa and closer to the former. It is not unusual that an antibody detects a band having different molecular weight than the predicted one so even the manufacturers sometimes mention this in their specifications. This is the case for instance with anti-TMEM16A antibodies SAB2102460 and SAB3500318 as bands were observed at 90 and 72 kDa, respectively. Also, with TMEM16A antibody (ab84115) the band appeared at 90 kDa instead of the predicted 114 kDa (http://www.abcam.com/tmem16a-antibody-ab84115.html). According to the manufacturer possible reasons for the difference include: post-translational modification, post-translation cleavage, splice variants, relative charge and multimers (e.g. dimerisation of a protein). This last one is usually prevented in reducing conditions, although strong interactions can result in the appearance of higher bands. The molecular weight of the protein band detected by anti-TMEM16A antibody (ab53213) used in the publication of Davis et al. showed tissue specificity as in murine portal vein it was below 80 kDa instead of the predicted size of 114 kDa which was the case for murine thoracic aorta and carotid artery [6]. Moreover, on murine portal vein samples the same antibody detected TMEM16A at around 160 kDa in a study of the same research group [7]. Exactly the same antibody however detected Ano1 at 149 and 139 kDa when used in brain and uterinal smooth muscle samples from mouse and human origin, respectively [8]. From these publications it seems that even the exactly same antibody can detect TMEM16A at different molecular weights on samples of various origin and even on the same tissues.

It must be highlighted that the antibodies used in our experiments were produced against human proteins which can be different from that of canine not only in sequence but also in molecular weight. According to our knowledge there are no publications made on canine cells/tissue describing the expression and molecular weight of either TMEM16A or Bestrophin-3. This interspecies difference however is unlikely as there were no major difference between molecular weights where TMEM16A was detected in human and canine tissues.

One explanation for the lower molecular weight can be isoform variations as for human TMEM16A three isoforms are known with molecular weights of 114, 98 and 74 kDa (http://www.uniprot.org/uniprot/Q5XXA6). The molecular weight of canine TMEM16A is 106 kDa (http://www.uniprot.org/uniprot/F1PQF9). Alternative splicing of TMEM16A has been reported previously in many tissues including the heart [9,10].

The TMEM16A antibody (H-41): Santa Cruz, sc-135235, used in our study recognizes a sequence that is present in each of the three isoforms, hence it is able to detect all of them. The band appeared in our experiments with TMEM16A antibody was lower than the predicted size of 114 kDa therefore it is unlikely that dimer formation of TMEM16A could occur. Nevertheless, not only homo- but also heterodimer formation of various TMEM16A isoforms was observed in murine portal vein [11].

Bestrophin-3

To test the specificity of anti-Bestrophin-3 antibody we performed Western blot experiments on canine left ventricular myocytes and human left ventricular tissue samples. As mentioned with TMEM16A, antibodies designed to recognize Bestrophin-3 can signal bands with other than the predicted molecular weight as for antibodies ab94904, Proteintech 20443-1-AP and ab123887. Regarding human Bestrophin-3 five isoforms has been described (http://www.uniprot.org/uniprot/Q8N1M1) but only four has been predicted in canine according to NCBI protein database. The five human isoforms have molecular weights of 76, 46, 8, 51 and 63 kDa. The shorter isoforms differ from the longest due to the lack of one or more parts of the full sequence. The antibody used in our experiments (Bestrophin-3 antibody (T-16): Santa Cruz, sc-70147, molecular weight: 47 kDa) recognizes and targets a sequence within a cytoplasmic domain but it is not specified where. According to our Western blots the bands between 100 and 130 kDa and 35 and 55 kDa were absent in the presence of the blocking peptide (not shown). The smaller size band is in the range of the size indicated by the manufacturer (47 kDa) and the antibody can bind to both the 46 and 51 kDa

isoforms. A possibility for the occurrence of Bestrophin-3 signal between 100 and 130 kDa on our Western blots is oligomerisation. Indeed, Bestrophins have been predicted to form dimers, tetramers or pentamers [12, 13] and Bestrophin-3 homodimer formation was confirmed [14]. The processing of samples (application of reducing conditions) can however destroy these oligomers and separate subunits from each other but strong interactions between isoforms or various proteins might remain intact.

To show the specificity of Bestrophin-3 antibody, parallel experiments were conducted using immunolabeling in the presence or the absence of the blocking peptide with exactly the same recording settings (gain, time of acquisition, pixel size etc…) during confocal imaging (Supplementary Fig. 2B). Only those isolated canine left ventricular myocytes cells showed striated pattern of green fluorescence (suggesting the presence of Bestrophin-3), where the specific blocking peptide was not used during the procedure. Those cells, however, where Bestrophin-3 antibody was used together with the blocking peptide during the procedure show barely detectable green color and only blue DAPI staining of nuclei was visible.

Table 1

$I_{9\text{-}AC}$ peaks measured by APVC under various experimental conditions

Condition	Early outward peak (A/F)	Late inward peak (A/F)	n
Control chloride, 1 Hz (47 mmol/L $[Cl^-]_{pipette}$)	**1.62±0.08**	**−0.16±0.03**	**15**
Control chloride, 1 Hz 10 mmol/L EGTA in pipette	1.17±0.09	−0.13±0.02	9
Control chloride, 1 Hz 10 mmol/L BAPTA in pipette	0.13±0.10	−0.08±0.02	6
Low chloride, 1 Hz (27 mmol/L $[Cl^-]_{pipette}$)	2.44±0.27	−0.06±0.03	4
Control chloride, 1 Hz	1.67±0.12	−0.12±0.02	5
Control chloride, 2 Hz	2.07±0.19	−0.15±0.02	5
Control chloride, 1 Hz 10 nmol/L isoproterenol	3.10±0.21	−0.36±0.11	6
Control chloride, 1 Hz 20 nmol/L Bay K8644	2.86±0.15	−0.30±0.03	8
Control chloride, 1 Hz 10 μmol/L ryanodine	1.05±0.03	−0.07±0.03	4

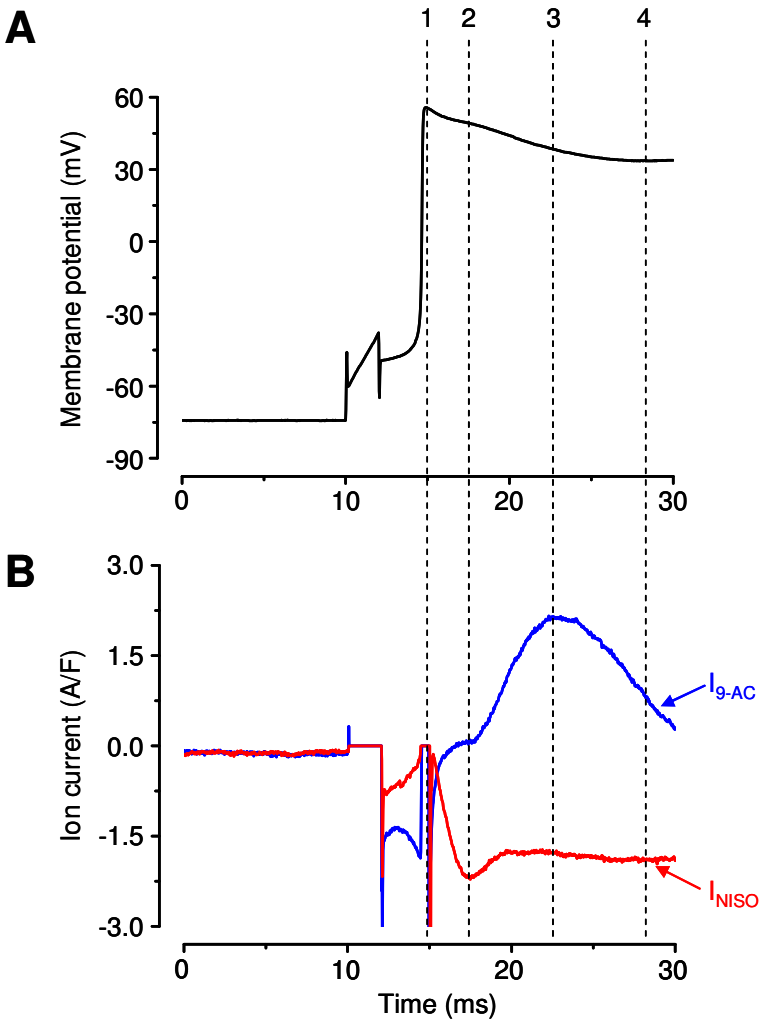

Supplementary Fig. 1 Temporal alignment of $I_{9\text{-}AC}$ and I_{NISO} measured with sequential APVC. Representative membrane potential (A) and current traces (B) measured on the same cell showing the first 15 ms of the AP. During the experiment the application of 9-AC was followed by the application of nisoldipine. $I_{9\text{-}AC}$ (0.5 mmol/L 9-AC-sensitive current) is illustrated with blue while I_{NISO} trace (1 µmol/L nisoldipine-sensitive current, including $I_{Ca,L}$ and Na^+/Ca^{2+} exchange current as two main components) is shown in red. Vertical dashed lines are placed at the peak of the AP (line 1), inward peak of I_{NISO} (line 2), outward peak of $I_{9\text{-}AC}$ (line 3) and at the end of phase-1 repolarization (line 4).

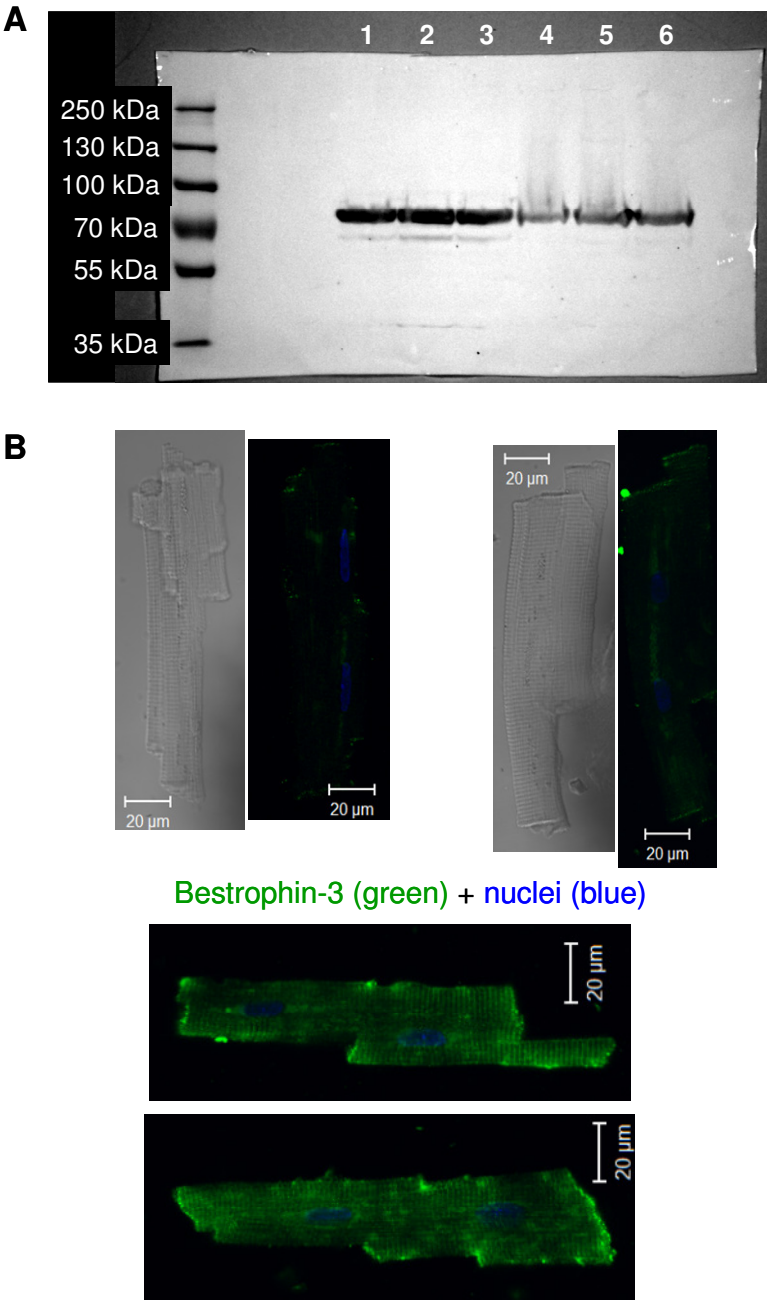

Supplementary Fig. 2 Specificity of antibodies used to detect TMEM16A and Bestrophin-3 proteins. (A) Representative full length Western blot image made with the primary antibody against TMEM16A (Santa Cruz Biotechnology, sc-135235, predicted molecular weight: 114 kDa.). Lanes 1-6 are isolated ventricular myocytes obtained from various layers of two canine left ventricles.
(B) Images taken from four canine left ventricular cells using exactly the same recording settings (gain, time of acquisition, pixel size etc…) during confocal imaging in the presence (upper four images) or the absence (lower two images) of the blocking peptide (Santa Cruz Biotechnology, sc-70147-P) against the Bestrophin-3 antibody (Santa Cruz Biotechnology, sc-70147). Left images in the upper pairs show the two cells using transmitted light of the confocal microscope and the right ones show nuclear staining in blue and very weak Bestrophin-3 staining (in green color) on the same cells. On the lowest two images, obtained without using the blocking peptide, striated labeling pattern can be observed.

A

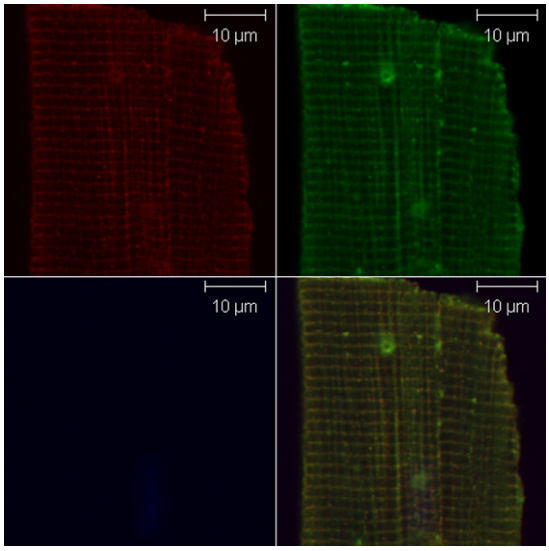

$Ca_v1.2$ (red) + Bestrophin-3 (green) + nuclei (blue) + Merged

B

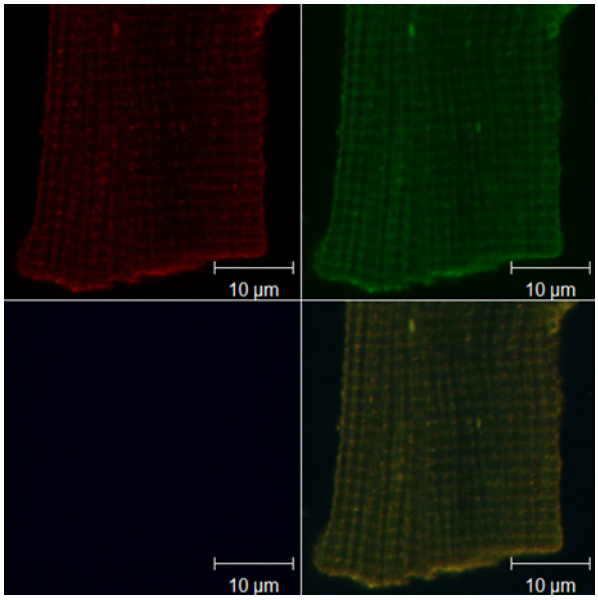

TMEM16A (red) + Bestrophin-3 (green) + nuclei (blue) + Merged

Supplementary Fig. 3 Confocal images showing the expression pattern of $Ca_v1.2$, TMEM16A, and Bestrophin-3 in canine ventricular myocytes.
(A) Expression of $Ca_v1.2$, Bestrophin-3, and nuclear staining in red (upper left), green (upper right), and blue (lower left), respectively. The lower right panel represents the overlay of the three images. Images depict approximately the upper 20 % of the cell presented on Fig. 7A.
(B) Expression of TMEM16A, Bestrophin-3, and nuclear staining in red (upper left), green (upper right), and blue (lower left), respectively. The lower right panel represents the overlay of the three images. Images show approximately the lower 25 % of the cell presented on Fig. 7B.

A

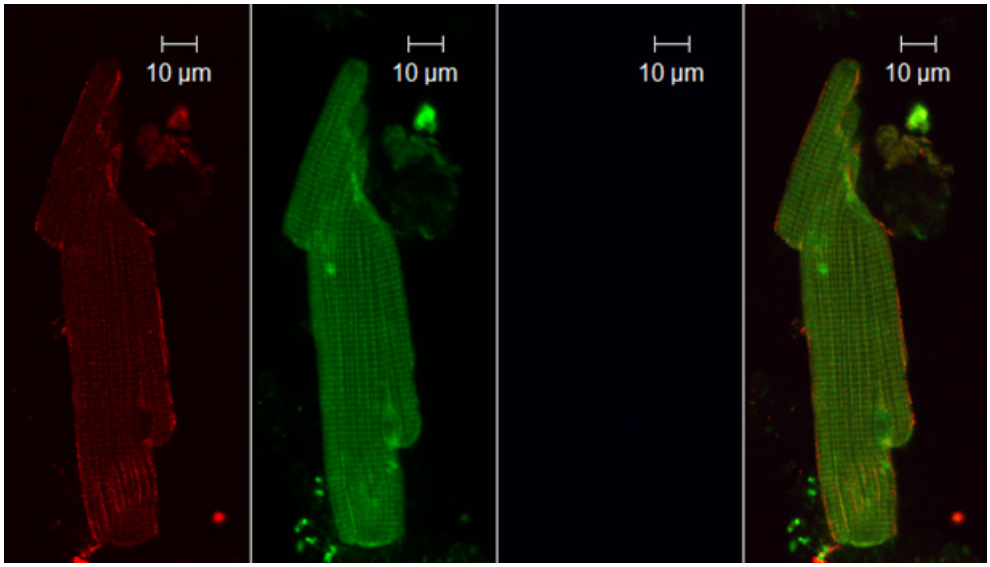

Cytochrome c (red) + TMEM16A (green) + nuclei (blue) + Merged

B

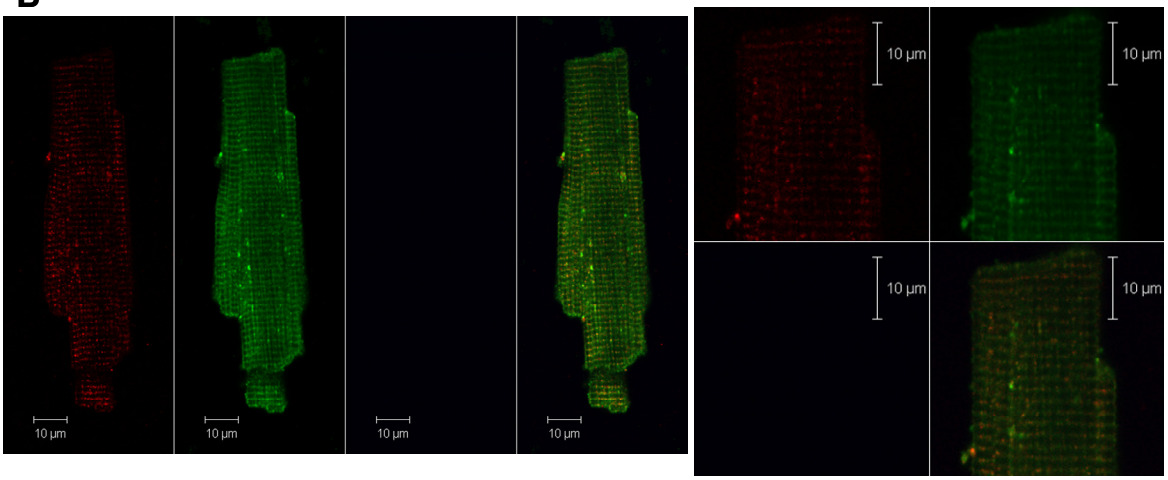

RyR (red) + Bestrophin-3 (green) + nuclei (blue) + Merged

Supplementary Fig. 4 Expression patterns of TMEM16A, Bestrophin-3, RyR and cytochrome c in canine ventricular myocytes.
(A) Representative cell showing the expression of cytochrome c, TMEM16A, and nuclear staining in red, green, and blue, respectively, from left to right. The far right panel represents the overlay of the three images.
(B) Representative cell showing the expression of RyR, Bestrophin-3, and nuclear staining in red, green, and blue, respectively from left to right and the overlay of these three images. Enlarged images made from the upper half of the same cell are represented on the right side.

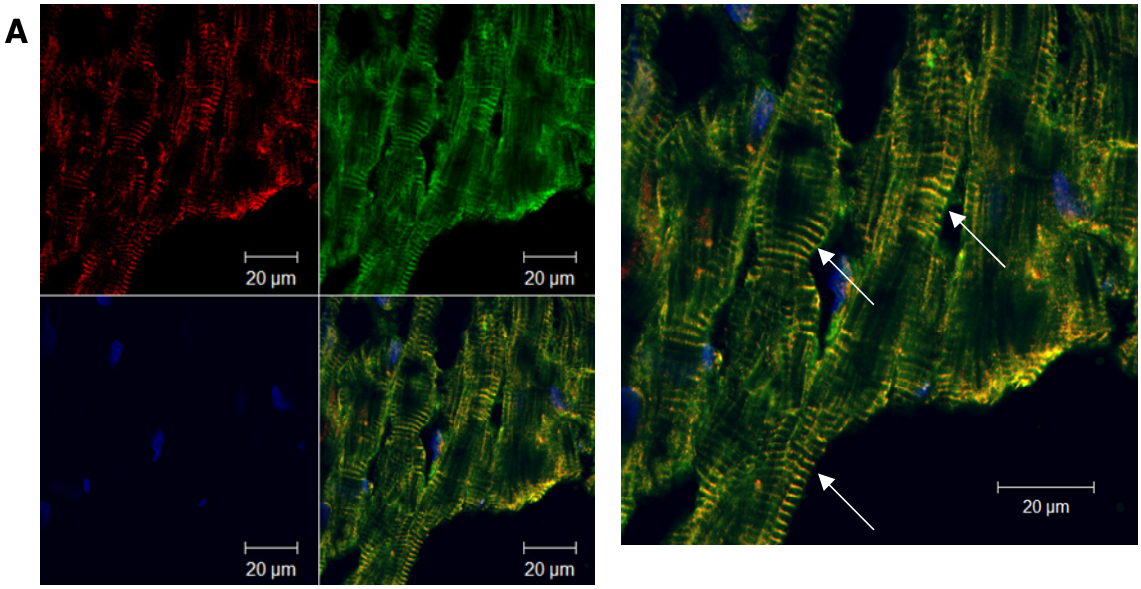

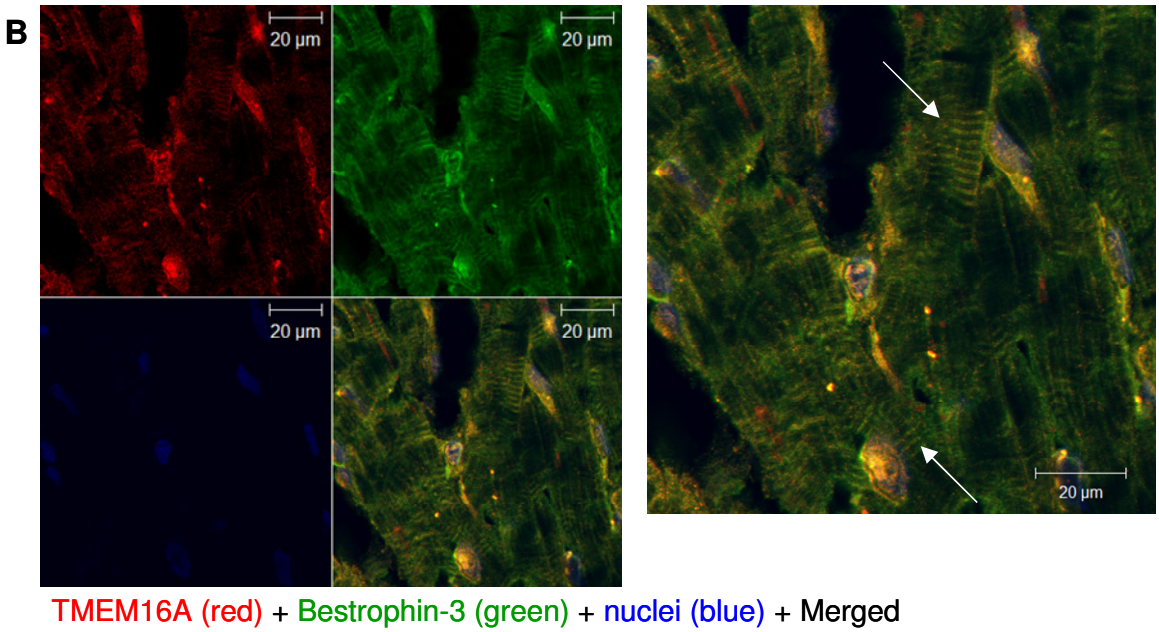

Supplementary Fig. 5 Confocal images showing the expression pattern of $Ca_v1.2$, TMEM16A, and Bestrophin-3 in non-diseased human left ventricular tissues.
(A) Representative images showing the expression of $Ca_v1.2$, Bestrophin-3, and nuclear staining in red (upper left), green (upper right), and blue (lower left), respectively. The lower right panel represents the overlay of the three images and enlarged on the right. White arrows point to some striations.
(B) Representative image showing the expression of TMEM16A, Bestrophin-3, and nuclear staining in red (upper left), green (upper right), and blue (lower left), respectively. The lower right panel represents the overlay of the three images and enlarged on the right. White arrows point to some striations.

Supplemental References

1. Vaczi K, Hegyi B, Ruzsnavszky F, Kistamas K, Horvath B, Banyasz T, et al. 9-Anthracene carboxylic acid is more suitable than DIDS for characterization of calcium-activated chloride current during canine ventricular action potential. Naunyn Schmiedebergs Arch Pharmacol 2015; 388: 87-100. doi: 10.1007/s00210-014-1050-9
2. Jost N, Virág L, Comtois P, Ordög B, Szuts V, Seprényi G, et al. Ionic mechanisms limiting cardiac repolarization reserve in humans compared to dogs. J Physiol 2013; 591: 4189-4206. doi: 10.1113/jphysiol.2013.261198.
3. MaxChelator calculation: http://web.stanford.edu/~cpatton/maxc.html
4. Banyasz T, Horvath B, Jian Z, Izu LT, Chen-Izu Y. Sequential dissection of multiple ionic currents in single cardiac myocytes under action potential-clamp. J Mol Cell Cardiol 2011; 50: 578-581. doi: 10.1016/j.yjmcc.2010.12.020.
5. Horvath B, Banyasz T, Jian Z, Hegyi B, Kistamas K, Nanasi PP, et al. Dynamics of the late Na+ current during cardiac action potential and its contribution to afterdepolarizations. J Mol Cell Cardiol 2013; 64: 59-68. doi: 10.1016/j.yjmcc.2013.08.010.
6. Davis AJ, Forrest AS, Jepps TA, Valencik ML, Wiwchar M, Singer CA, et al. Expression profile and protein translation of TMEM16A in murine smooth muscle. Am J Physiol Cell Physiol 2010; 299: C948-59. doi: 10.1152/ajpcell.00018.2010.
7. Sones WR, Davis AJ, Leblanc N, Greenwood IA. Cholesterol depletion alters amplitude and pharmacology of vascular calcium-activated chloride channels. Cardiovasc Res 2010; 87: 476-84. doi: 10.1093/cvr/cvq057.
8. Bernstein K, Vink JY, Fu XW, Wakita H, Danielsson J, Wapner R, et al. Calcium-activated chloride channels anoctamin 1 and 2 promote murine uterine smooth muscle contractility. Am J Obstet Gynecol 2014; 211: 688.e1-10. doi: 10.1016/j.ajog.2014.06.018.
9. Ferrera L, Caputo A, Ubby I, Bussani E, Zegarra-Moran O, Ravazzolo R, et al. Regulation of TMEM16A chloride channel properties by alternative splicing. J Biol Chem 2009; 284: 33360-8. doi: 10.1074/jbc.M109.046607.
10. O'Driscoll KE, Pipe RA, Britton FC. Increased complexity of Tmem16a/Anoctamin 1 transcript alternative splicing. BMC Mol Biol 2011; 12: 35. doi: 10.1186/1471-2199-12-35.
11. Ohshiro J, Yamamura H, Saeki T, Suzuki Y, Imaizumi Y. The multiple expression of Ca2+-activated Cl- channels via homo- and hetero-dimer formation of TMEM16A splicing variants in murine portal vein. Biochem Biophys Res Commun 2014; 443: 518-23. doi: 10.1016/j.bbrc.2013.11.117.
12. Sun H, Tsunenari T, Yau KW, Nathans J. The vitelliform macular dystrophy protein defines a new family of chloride channels. Proc Natl Acad Sci U S A 2002; 99: 4008-13. doi:10.1073/pnas.052692999
13. Stanton JB, Goldberg AF, Hoppe G, Marmorstein LY, Marmorstein AD. Hydrodynamic properties of porcine bestrophin-1 in Triton X-100. Biochim Biophys Acta 2006; 1758: 241-7. doi:10.1016/j.bbamem.2006.01.024
14. Bharill S, Fu Z, Palty R, Isacoff EY. Stoichiometry and specific assembly of Best ion channels. Proc Natl Acad Sci U S A 2014; 111: 6491-6. doi: 10.1073/pnas.1400248111